MOX-Report No. 11/2016

Isogeometric Analysis and proper orthogonal decomposition for the acoustic wave equation

Zhu, S.; Dedè, L.; Quarteroni, A.

Isogeometric analysis and proper orthogonal decomposition for the acoustic wave equation[*]

Shengfeng Zhu[†], Luca Dedè[‡], and Alfio Quarteroni[‡§]

January 27, 2016

Abstract

Isogeometric Analysis (IGA) is used in combination with proper orthogonal decomposition (POD) for model order reduction of the time parameterized acoustic wave equations. We propose a fully discrete IGA-Newmark-POD approximation and we analyze the associated numerical error, which features three components due to spatial discretization by IGA, time discretization with the Newmark scheme, and modes truncation by POD. We prove stability and convergence. Numerical examples are presented to show the accuracy and efficiency of IGA-based POD techniques for the model order reduction of the acoustic wave equation.

Keywords: Isogeometric Analysis, Proper orthogonal decomposition, Reduced order modeling, Acoustic wave equation

Mathematics Subject Classification. 65M12, 65M15, 65M60

1 Introduction

Proper orthogonal decomposition (POD) is a popular reduced order modeling (ROM) technique to solve problems of Engineering interest (see e.g. [6, 40]). The method is also known as principle component analysis in Statistics and Karhunen-Loève expansion in stochastic analysis [21]. POD techniques have been applied in various fields of computational mechanics for ROM of physical, geometric and/or time parameterized steady and unsteady partial differential equations (PDEs); see e.g. [18, 31, 35, 40] and the references therein.

POD-Galerkin methods for parameterized PDEs can be regarded as ROM for the solution manifolds depending on parameters [20, 26, 24, 27, 29]. In this case, we will address the case of a time dependent acoustic wave equation and we will let the time play the role of parameter. For unsteady PDEs with time variable being the parameter, Kunisch and Volkwein analyzed the convergence of POD-Galerkin methods under a unified framework for problems including heat, Burgers [26], and Navier-Stokes equations [27]. POD-Galerkin methods are developed in [2, 8, 19] for ROM of wave equations. The *method of snapshots* in POD-Galerkin methods chooses discrete instances in the parameter domain and uses the corresponding field variables (i.e. the snapshots) to obtain a low-dimensional basis [26, 33, 39]. The generation of the snapshots is the first crucial step in POD-Galerkin reduced modeling of PDEs. For error estimates and generation of

[†]Corresponding author. Department of Mathematics and Shanghai Key Laboratory of Pure Mathematics and Mathematical Practice, East China Normal University, Shanghai, 200241, China. E-mail: sfzhu@math.ecnu.edu.cn.

[‡]CMCS-Chair of Modeling and Scientific Computing, MATHICSE-Mathematics Institute of Computational Science and Engineering, EPFL-École Polytechnique Fédérale de Lausanne, Station 8, CH-1015, Lausanne, Switzerland. E-mail: luca.dede@epfl.ch; alfio.quarteroni@epfl.ch.

[§]MOX-Modeling and Scientific Computing, Department of Mathematics, Politecnico di Milano, Piazza L. da Vinci 32, I-20133, Milano, Italy.

the POD-basis proposed in [26, 27], the snapshots are often assumed to be "exact" regardless of the spatial discretization.

However, "exact" snapshots are usually not available in practice and instead "very accurate", but still approximate snapshots, the so-called *truth* (or *high fidelity*) *approximations* [39], are considered. Most of the existing methods of snapshots for ROM of unsteady PDEs thus need to compute snapshots numerically by fully discrete approximations, such as backward Euler or Crank-Nilcolson scheme for time discretization and the popular *Finite Element Method* (FEM) for spatial discretization (see e.g., [8, 25, 26, 29, 36, 24]). As a popular ROM technique, POD is usually designed to capture the information contained in the set of snapshots in the sense of least-squares. This does not necessarily imply that the reduced order space spanned by the POD basis performs well in approximating the solution space (or manifold) of the PDE since the snapshots are "approximate" [18]. Actually, the error between the POD-Galerkin solution and the exact solution consists of two components: the space-time full discretization and the POD eigenvalue truncation, respectively. For clarity, let us assume that u is an exact solution of a given PDE and denote by u_s and u_r an approximate (high fidelity) snapshot and a POD solution, respectively. We have, in some suitable norm $\| \cdot \|$ [41, 18]:

$$\underbrace{\|u - u_r\|}_{\text{Total error}} \leq \underbrace{\|u - u_s\|}_{\text{Snapshot error}} + \underbrace{\|u_s - u_r\|}_{\text{POD error}} \tag{1}$$

by the triangle inequality. In this respect, POD deals with the reduction of the *POD error* $\|u_s - u_r\|$ by means of modal analysis and eigenmodes truncation. Therefore, to make the *snapshot error* $\|u - u_s\|$ and hence the *total error* $\|u - u_r\|$ small, we need good "approximate" snapshots to begin with. Motivated by this request, we choose in this paper *Isogeometric Analysis* (IGA) [9, 22] to obtain our snapshots in place of FEM. The motivation stems from the fact that the IGA has shown advantages over FEM on accuracy and efficiency in ROM [41].

Nowadays, IGA has been successfully applied in various fields including structural mechanics, fluid dynamics, acoustics, electromagnetism; see e.g. [3, 4, 7, 9, 13, 14, 34, 37]. IGA represents a generalization of the *isoparametric* FEM for which *Non-Uniform Rational B-spline* (NURBS) basis functions, a standard tool in Computer-Aided Design, can first be used for the geometrical representation of the computational domain and then as base for the finite-dimensional trial spaces of the approximate solutions to the PDEs. It follows that IGA possesses a significant geometrical advantage in several circumstances since several computational domains of practical interest, such as freeform and sculptured surfaces and conic sections, are exactly represented by NURBS. In these cases, the geometrical representation allowed by FEM typically introduces numerical errors, which may lead to a loss of accuracy of the method [41, 4, 9, 10, 22]. Thus, in these cases the accuracy of numerical solutions is generally enhanced by IGA compared with FEM. Then, NURBS-based IGA possesses the advantage of yielding highly accurate approximations to the smooth solutions of PDEs when using basis functions more regular than globally C^0-continuous. In particular, the global regularity of the NURBS basis functions can be enhanced up to C^{p-1}-continuous, with p denoting the degree of the piecewise polynomials used in their construction. This can be realized by a special refinement called *k-refinement* (typical of NURBS) differently from $h-$ and $p-$ refinements.

The considerations above motivate us to use IGA in POD-Galerkin methods for ROM of unsteady PDEs. For IGA-ROM approximation of parabolic equations, both accuracy and efficiency can be achieved as proven in [41]. For the error due to spatial discretization, IGA is expected to be more accurate than FEM for approximating smooth solutions of PDEs [9, 10, 22, 5, 15, 23, 37]. The solutions to the acoustic wave equations are closely related to the corresponding elliptic eigenvalue problems by separation of variables and modal analysis [12]. In eigenvalue problems the regular basis functions are significantly better than their C^0-continuous counterpart for modal analysis [10, 14, 23]. Thus, IGA with more regular basis functions is more accurate than FEM for obtaining truth approximation of acoustic wave equations. This advantage may also be relevant in the context of the POD-Galerkin method which is based on modal analysis and

eigenvalue truncation as shown in [41]. For this reason, together with the exactness of the geometrical representation, the use of IGA with NURBS basis functions which are C^{p-1}-continuous can be significantly beneficial for POD-Galerkin methods both in terms of accuracy and efficiency.

Acoustic wave equations, as basic hyperbolic PDEs, have many applications and thus are fundamentally important in Engineering [12]. Reduction is operated with the purpose of lowering the computational complexity of the numerical approximation to the acoustic wave equation. In this respect, the time variable is the only parameter that is addressed in the reduction process; it is well-known that dealing with hyperbolic problems, special care should be devoted to achieve efficient ROM when considering the multiparameter case [1, 11, 38]. In this paper, we use IGA rather than FEM [2, 8, 19] to obtain truth approximations for ROM of acoustic wave equations and we propose a fully IGA-Newmark-POD Galerkin scheme for their approximation. We split the error of the POD-Galerkin solution into two parts as in Eq. (1) and show that both the accuracy of truth approximation and POD truncation are important for obtaining accuracy and efficiency in ROM. We analyze the stability and convergence of the discrete schemes by *a priori* error estimates. Numerical experiments are performed to show advantages of IGA used as truth approximations both with respect to the "exact" geometrical representation of computational domains of practical interest and the use of smooth basis functions allowed by NURBS. These advantages are shown to be usefull for enhancing accuracy and efficiency in ROM by POD.

The paper is organized as follows. In Section 2, we first introduce the essential formulations of IGA for the spatial discretization of PDEs. Then, the IGA semi-discrete and fully space-time (with Newmark scheme) discretization methods are presented; stability and convergence analysis for acoustic wave equations are carried out. In Section 3, we recall the POD methods for ROM of unsteady PDEs with the time variable as parameter. In Section 4, we present the IGA-POD Galerkin scheme and show its stability and convergence properties by performing *a priori* error estimates. Numerical aspects and the algorithm are detailed. In Section 5, we give numerical examples to show effectiveness and advantages of our approach. Finally, conclusions follow.

2   IGA for acoustic wave equations

In this section, we first introduce the wave equation model in acoustics. We introduce B-splines and NURBS for the formulation of IGA. Then, we propose a spatial discretization scheme by IGA and temporal discretization using the Newmark-scheme. We discuss the stability and convergence of the schemes.

2.1   Problem formulations

Let $\Omega \subset \mathbb{R}^d$ $(d = 2, 3)$ be an open bounded domain with Lipschitz continuous boundary $\partial\Omega$. We indicate by $L^2(\Omega)$ the Hilbert space of measurable functions that are square integrable. The L^2 inner product and the corresponding norm are denoted by $(\cdot, \cdot)$ and $\| \cdot \|$, respectively. Denote $H^1(\Omega) := \{v \in L^2(\Omega) \,|\, D_i v \in L^2(\Omega), i = 1, \ldots, d\}$ with D_i being the partial distributional derivative with respect to x_i and $H^1_{\Gamma_D}(\Omega) := \{v \in H^1(\Omega) \,|\, v = 0 \text{ on } \Gamma_D\}$ with dual space denoted by $H^{-1}_{\Gamma_D}(\Omega)$. Denote by $(\cdot, \cdot)_k$ the scalar or vectorial H^k inner product and define the corresponding norm $\|v\|_k := \sqrt{(v, v)_k}$. We will need the Hilbert space $H^k(\Omega)$, for k a non-negative integer. Accordingly, $(\cdot, \cdot)_k$, $\| \cdot \|_k$ and $| \cdot |_k$ will be used as their scalar inner products, norms and seminorms, respectively.

We consider the acoustic wave equation

$$
\begin{cases}
u_{tt} - \Delta u = f & \text{in } \Omega \times (0, T], \\
u = g_D & \text{on } \Gamma_D \times (0, T], \\
\nabla u \cdot n = g_N & \text{on } \Gamma_N \times (0, T], \\
u = u_0 & \text{in } \Omega \times \{0\}, \\
u_t = v_0 & \text{in } \Omega \times \{0\},
\end{cases}
\tag{2}
$$

with $T > 0$. We define the bilinear form $a(\cdot, \cdot) \colon V \times V \to \mathbb{R}$ as:

$$
a(u, v) := \int_\Omega \nabla u \cdot \nabla v \, \mathrm{d}x \quad \forall u, v \in V.
\tag{3}
$$

By the Cauchy-Schwarz inequality, we have that

$$
|a(u, v)| \leq \|u\|_1 \|v\|_1 \quad \forall u, v \in V
\tag{4}
$$

and by the Poincaré inequality there exists a constant $0 < \alpha < 1$ such that (e.g., [32]):

$$
|a(v, v)| \geq \alpha \|v\|_1^2 \quad \forall v \in V.
\tag{5}
$$

We use the abbreviations $H := L^2(\Omega)$ and $V := H^1_{\Gamma_D}(\Omega)$ with dual space V^*. With this notation, we define the space-time function spaces $\mathcal{H} := L^2(0, T; H)$, $\mathcal{V} := \{v \in L^2(0, T; V) | v_t \in \mathcal{H}\}$ and

$$
\widehat{\mathcal{V}} := \{v \in \mathcal{V} | v \in C([0, T]; V), v_t \in C([0, T]; H), v_{tt} \in L^2(0, T; V^*)\}
\tag{6}
$$

We denote with $L^2(0, T; V)$ the space of measurable functions $\phi : (0, T) \to V$, which are square integrable, i.e., $\int_0^T \|\phi(t)\|_V^2 \mathrm{d}t < \infty$, where $\phi(t) := \phi(t, \cdot)$ is considered as a function of the space variable only for t fixed.

Given $f \in L^2(0, T; H^{-1}_{\Gamma_D}(\Omega))$, $u_0 \in V$, and $v_0 \in H$, the weak formulation of problem (2) reads: for $t \in (0, T]$, find $u \in \widehat{\mathcal{V}}$ such that

$$
(u_{tt}(t), w) + a(u(t), w) = (f(t), w) + (g_N, w) \quad \forall \, w \in V,
\tag{7}
$$
$$
(u(0), w) = (u_0, w) \quad \forall w \in L^2(\Omega),
\tag{8}
$$
$$
(u_t(0), w) = (v_0, w) \quad \forall w \in L^2(\Omega),
\tag{9}
$$

which admits a unique weak solution $u \in \mathcal{V} \cap C([0, T]; V)$ with $u_t \in \mathcal{H} \cap C([0, T]; H)$ and $u_{tt} \in L^2(0, T; V^*)$ (see e.g. [12]).

2.2 IGA space semi-discretization of PDE model

Let us introduce a spatial semi-discretization of (7) based on IGA [9]. We recall in the following some basic definitions and properties of IGA.

2.3 B-splines and NURBS

We recall univariate B-splines and NURBS [30]. For any α ($1 \leq \alpha \leq d$) and positive integers m_α and n_α, we define the *knot vector* $\Xi_\alpha := \{0 = \xi_{1,\alpha}, \xi_{2,\alpha}, \ldots, \xi_{n_\alpha + p_\alpha + 1, \alpha} = 1\}$ consisting of nondecreasing *knots*, i.e., $\xi_{1,\alpha} \leq \xi_{2,\alpha} \leq \ldots \leq \xi_{n_\alpha + p_\alpha + 1, \alpha}$. Knots may be repeated with the number of repetitions called *multiplicity*. A knot vector is assumed to be *open*, i.e., both of the first and the last $p_\alpha + 1$ knots are repeated, where p_α is the polynomial degree. Denote by $B_{i,\alpha}$ ($i = 1, 2, \ldots, n_\alpha$) the *B-spline* basis functions, which can be

produced by the recursive Cox-de Boor formula [30]. Each B-spline basis function is everywhere pointwise C^∞-continuous except at knots $\xi_{i,\alpha}$, where it is $C^{p_\alpha - \kappa_{i,\alpha}}$-continuous if the multiplicity of the knot is $\kappa_{i,\alpha}$ with $1 \leq \kappa_{i,\alpha} < p_\alpha + 1$. The B-spline basis functions are non-negative, locally supported in $(\xi_{i,\alpha}, \xi_{i+p_\alpha+1,\alpha})$ (the *knot span*), and constitute a partition of unity [22], i.e. $\sum_{i=1}^{n_\alpha} B_{i,\alpha} = 1$. We define the space of univariate B-splines $\mathcal{B}_\alpha \equiv \mathcal{B}(\Xi_\alpha; p_\alpha) := \mathrm{span}\{B_{i,\alpha}\}_{i=1,\dots,n_\alpha}$.

Multivariate tensor product B-splines are defined based on d knot vectors Ξ_α, $\alpha = 1, \dots, d$. Let $\widehat{\Omega} := (0,1)^d \subset \mathbb{R}^d$ be an open *parametric domain*. The knot vectors partition $\widehat{\Omega}$ into "mesh" elements, which constitute a mesh $\mathcal{Q}_h \equiv \mathcal{Q}_h(\Xi_1, \dots, \Xi_d) := \{Q = \otimes_{\alpha=1}^d (\xi_{i_\alpha,\alpha}, \xi_{i_\alpha+1,\alpha}) \mid p_\alpha + 1 \leq i_\alpha \leq n_\alpha - 1\}$. Let us denote $\widehat{h}_Q := \mathrm{diam}(Q)$ for all $Q \in \mathcal{Q}_h$ and the global mesh size $\widehat{h} := \max_{Q \in \mathcal{Q}_h}\{\widehat{h}_Q\}$. For notational convenience, we denote a multi-index $\boldsymbol{i} := (i_1, \dots, i_d)$ and a corresponding multi-index set $I := \{\boldsymbol{i} = (i_1, \dots, i_d) \mid 1 \leq i_\alpha \leq n_\alpha \text{ for } 1 \leq \alpha \leq d\}$. Then, for each multi-index $\boldsymbol{i} \in I$, we define the tensor product B-spline basis functions $B_{\boldsymbol{i}} : \widehat{\Omega} \to \mathbb{R}$, $B_{\boldsymbol{i}} := B_{i_1,1} \otimes \dots \otimes B_{i_d,d}$ and corresponding tensor product B-splines space:

$$\mathcal{B}_h \equiv \mathcal{B}_h(\Xi_1, \dots, \Xi_d; p_1, \dots, p_d) := \mathrm{span}\{B_{\boldsymbol{i}}\}_{\boldsymbol{i} \in I}. \tag{10}$$

Notice that the functions in $\mathcal{B}_h$ are piecewise polynomials of degree p_α along each coordinate α.

We associate the basis functions $B_{\boldsymbol{i}}$ with positive weights $\omega_{\boldsymbol{i}}$ and define a *weighting function* $\omega : \widehat{\Omega} \to \mathbb{R}$, $\omega := \sum_{\boldsymbol{i} \in I} \omega_{\boldsymbol{i}} B_{\boldsymbol{i}}$. The NURBS basis functions on the parameter patch are defined by projection:

$$R_{\boldsymbol{i}} : \widehat{\Omega} \to \mathbb{R}, \quad R_{\boldsymbol{i}} = \frac{\omega_{\boldsymbol{i}} B_{\boldsymbol{i}}}{\omega} \tag{11}$$

and the corresponding NURBS space reads: $\mathcal{S}_h \equiv \mathcal{S}_h(\Xi_1, \dots, \Xi_d; p_1, \dots, p_d; \omega) := \mathrm{span}\{R_{\boldsymbol{i}}\}_{\boldsymbol{i} \in I}$.

In order to perform a parameterization of the physical domain, we introduce the control points $\mathbf{C}_{\boldsymbol{i}} \in \mathbb{R}^d$ and define the *geometric mapping* $\mathbf{F} : \widehat{\Omega} \to \Omega$ with $\mathbf{F} := \sum_{\boldsymbol{i} \in I} \mathbf{C}_{\boldsymbol{i}} R_{\boldsymbol{i}}$. Let us assume that $\mathbf{F}$ is invertible and possesses smooth inverse a.e. in each element $Q \in \mathcal{Q}_h$. We define $\nabla\mathbf{F} : \widehat{\Omega} \to \mathbb{R}^d$ and $J_{\mathbf{F}} : \widehat{\Omega} \to \mathbb{R}$ to be the Jacobian matrix and determinant of map $\mathbf{F}$, respectively. By using $\mathbf{F}$, we define a *physical mesh* in the physical domain Ω, whose elements are obtained as the image of the elements in the parametric domain, i.e., $\mathcal{K}_h := \{K = \mathbf{F}(Q) \mid Q \in \mathcal{Q}_h\}$. The corresponding mesh size in the physical domain is defined as $h := \max_{K \in \mathcal{K}_h} h_K$, where $h_K = \|\nabla\mathbf{F}\|_{L^\infty(Q)} h_Q$. Associated with a family of meshes $\{\mathcal{Q}_h\}_h$ in parametric domain $\widehat{\Omega}$, we introduce a family of meshes $\{\mathcal{K}_h\}_h$ in physical domain Ω.

Furthermore, we define the space spanned by NURBS basis functions in Ω as the push-forward of the space $\mathcal{S}_h$, which reads:

$$\mathcal{V}_h \equiv \mathcal{V}_h(p_1, \dots, p_\alpha) := \mathrm{span}\{R_{\boldsymbol{i}} \circ \mathbf{F}^{-1}\}_{\boldsymbol{i} \in I} = \mathrm{span}\{\mathcal{R}_{\boldsymbol{i}}\}_{\boldsymbol{i} \in I}, \tag{12}$$

where $\{\mathcal{R}_{\boldsymbol{i}}\}_{\boldsymbol{i} \in I}$ is the NURBS basis in the physical domain with $\mathcal{R}_{\boldsymbol{i}} := R_{\boldsymbol{i}} \circ \mathbf{F}^{-1}$ for all $\boldsymbol{i} \in I$. Let the degree p of piecewise B-spline polynomials be denoted by p and so that of NURBS be defined as $p := \min_{1 \leq \alpha \leq d}\{p_\alpha\}$.

We recall the interpolation theory of NURBS in [4] for obtaining interpolation error estimates of IGA. Given a function $\widehat{v} \in L^2(\widehat{\Omega})$, we define a *projective operator* over the B-splines space $\mathcal{B}_h$ as: $\Pi_{\mathcal{B}_h} : L^2(\widehat{\Omega}) \to \mathcal{B}_h$, $\Pi_{\mathcal{B}_h}\widehat{v} := \sum_{\boldsymbol{i} \in I} \varrho_{\boldsymbol{i}}(\widehat{v}) B_{\boldsymbol{i}}$, where the linear functionals $\varrho_{\boldsymbol{i}}(\widehat{v}) \in L^2(\widehat{\Omega})'$ determine the dual basis for the set of B-splines, i.e., they are such that $\varrho_{\boldsymbol{j}}(B_{\boldsymbol{i}}) = \delta_{\boldsymbol{i},\boldsymbol{j}}$ for $\boldsymbol{i}, \boldsymbol{j} \in I$, with δ the Kronecker function. The corresponding projective operator over the NURBS space $\mathcal{S}_h$ in $\widehat{\Omega}$ is defined by means of the NURBS basis functions in (11) through the weighting function ω, as:

$$\Pi_{\mathcal{S}_h} : L^2(\widehat{\Omega}) \to \mathcal{S}_h, \quad \Pi_{\mathcal{S}_h}\widehat{v} := \frac{\Pi_{\mathcal{S}_h}(\omega\widehat{v})}{\omega} \tag{13}$$

for all $\widehat{v} \in L^2(\widehat{\Omega})$. In this manner, the projective operator over $\mathcal{V}_h$, the NURBS space (12), is defined as the push-forward of the operator $\Pi_{\mathcal{S}_h}$

$$\Pi_{\mathcal{V}_h} : L^2(\Omega) \to \mathcal{V}_h, \quad \Pi_{\mathcal{V}_h} v := (\Pi_{\mathcal{S}_h}(\widehat{v}) \circ \mathbf{F}^{-1}. \tag{14}$$

Now let $\{Q_h\}_h$ and $\{K_h\}_h$ be regular and quasi-uniform families of meshes in the parameter and physical spaces, respectively. We recall the global interpolation error estimate of NURBS for IGA as follows ([4]).

Lemma 2.1 (Global interpolation error estimate)**.** *Given the integers ℓ and σ, with $0 \leq \ell \leq \delta$, $\delta = \min\{\sigma, p+1\}$, $\ell \leq k_{\mathrm{m}} + 1$, and $k_{\mathrm{m}} \geq 0$ the minimum regularity of basis functions (i.e. $C^{k_{\mathrm{m}}}$-continuous in Ω), we have:*

$$|u - \Pi_{\mathcal{V}_h} u|_\ell \leq C_1 h^{\delta-\ell} \|u\|_\sigma, \tag{15}$$

for any $u \in H^\sigma(\Omega)$, where the positive constant $C_1 = C_1(\|\nabla \boldsymbol{F}\|_{L^\infty(\widehat{\Omega})}, k_{\mathrm{m}})$ only depends on k_{m} and the shape of Ω, but not on its size.

Based on the local inverse inequality in [4], one obtains (see [41]):

Lemma 2.2 (Global inverse inequality)**.** *Let k and l be two integers such that $0 \leq k \leq l$, then we have*

$$\|v_h\|_l \leq C_2 h^{k-l} |v_h|_k \quad \forall v_h \in \mathcal{V}_h, \tag{16}$$

with $C_2 = C_2(\Omega, \|\nabla \boldsymbol{F}\|_{L^\infty(\widehat{\Omega})}, k_{\mathrm{m}}) > 0$.

2.4 Spatial semi-discretization of IGA for the acoustic wave equation

Let V_h be the finite-dimensional subspace of V reading $V_h = V \cap [\mathcal{V}_h]^d$. Without loss of generality, consider the case with $\Gamma_N = \varnothing$. A general spatial semi-discrete Galerkin approximation of (7)-(9) reads: for any given $t \in (0, T]$, find $u_h(t) \in V_h$ such that

$$\begin{cases} (u_{h,tt}(t), v_h) + a(u_h(t), v_h) = (f(t), v_h) & \forall v_h \in V_h \\ u_h(0) = u_{0,h}, \\ u_{h,t}(0) = v_{0,h}, \end{cases} \tag{17}$$

where $u_{0,h}$ (or $v_{0,h}$) is some approximation of u_0 (or v_0) obtained by interpolation or L^2 projection onto $\mathcal{V}_h$.

Let us first define an *elliptic projection* operator $P_h : V \to V_h$ for each $v \in V$:

$$a(P_h v, v_h) = a(v, v_h) \quad \forall v_h \in V_h, \tag{18}$$

from which we obtain the Galerkin orthogonality:

$$a(v - P_h v, v_h) = 0 \quad \forall v_h \in V_h. \tag{19}$$

We recall the following result from [41].

Lemma 2.3. *Let $\{Q_h\}_h$ be a regular and quasi-uniform family of meshes. Then, there exists a positive constant $C_3 = C_3(\|\nabla \boldsymbol{F}\|_{L^\infty(\widehat{\Omega})}, \alpha, k_{\mathrm{m}})$ independent of h such that*

$$\|v - P_h v\| + h\|v - P_h v\|_1 \leq C_3 h^{p+1} |v|_{p+1} \quad \forall v \in H^{p+1}(\Omega) \cap V. \tag{20}$$

Then, we have the error estimate between exact solution $u(t)$ and spatial semi-discrete approximation $u_h(t)$.

Lemma 2.4. *Let the hypotheses of Lemma 2.3 hold. In addition, let us assume that $f \in C^0([0, T]; L^2(\Omega))$, $u_0 \in H^{p+1}(\Omega)$ with $p \geq 1$, and that the solution u of (7) is such that $u \in C^0([0, T]; H^{p+1}(\Omega))$ and $u_t \in L^2(0, T; H^{p+1}(\Omega))$. Then, by using piecewise polynomials of degree less than or equal to p in definition of NURBS space $\mathcal{V}_h$, the solutions u and u_h to (7) and (17), respectively, satisfy*

$$\|u(t) - u_h(t)\| + h|u(t) - u_h(t)|_1 + \|u_t(t) - u_{h,t}(t)\|$$
$$\leq C_4 h^{p+1} \left(\|u(t)\|_{p+1} + \|u_t(t)\|_{p+1} + \int_0^t \|u_{tt}\|_{p+1} \, \mathrm{d}s \right) \tag{21}$$

for each $t \in [0, T]$ with $C_4 = C_4(\|\nabla \boldsymbol{F}\|_{L^\infty(\widehat{\Omega})}, \alpha, k_{\mathrm{m}})$ some positive constant independent of h.

6

Proof. The proof follows from the FEM version of space semi-discretization (see e.g. [17], [28] and [32]). $\square$

2.5 Full space-time discretization of PDE model

We now apply the Newmark scheme for the time discretization of problem (17) (see e.g. [28]). For $N_t \in \mathbb{N}$, we introduce a time step $\tau = T/N_t$ and uniform discrete time instances $t_n = n\tau$ for $n = 0, 1, \ldots, N_t$. Let us denote $u^n := u(t_n)$ and $f^n := f(t^n)$, $n = 0, \ldots, N_t$. For notational simplification, the superscript "$n \pm 1/2$" of an arbitrary quantity, e.g. ζ, means that $\zeta^{n\pm1/2} := (\zeta^{n\pm1} + \zeta^n)/2$ with $\zeta^n := \zeta(t_n)$. Thus, $(\zeta^{n-1} + 2\zeta^n + \zeta^{n+1})/4 = (\zeta^{n-1/2} + \zeta^{n+1/2})/2$. Let D_τ^+ and D_τ^- be the forward and backward finite difference operators, respectively:

$$D_\tau^+ \zeta^n := \frac{\zeta^{n+1} - \zeta^n}{\tau} \quad \text{and} \quad D_\tau^- \zeta^n := \frac{\zeta^n - \zeta^{n-1}}{\tau}.$$

Thus, $D_\tau^+ D_\tau^- u_h^n = (u_h^{n-1} - 2u_h^n + u_h^{n+1})/\tau^2$. Note that here $u_h^n \simeq u_h(t_n)$. Then, we have the following IGA-Newmark full space-time discretization scheme: for $n = 1, \ldots, N_t - 1$, find $u_h^{n+1} \in V_h$ such that

$$\begin{cases} \left(D_\tau^+ D_\tau^- u_h^n, w_h\right) + \frac{1}{2}a\left((u_h^{n-1/2} + u_h^{n+1/2}), w_h\right) = (f^n, w_h) \quad \forall w_h \in V_h \\ u_h^0 = u_{0,h}, \quad v_h^0 = v_{0,h}, \end{cases} \tag{22}$$

where v_h^0 is the initial velocity approximation. We use (22) with $n = 0$ and the initial derivative approximation $(u_h^1 - u_h^{-1})/(2\tau) = v_{0,h}$ to cancel u_h^{-1} and compute u_h^1 from u_h^0. The Newmark scheme is unconditionally stable and second order accurate in time. We propose the following *a priori* error estimates for the fully-discrete approximation.

Lemma 2.5. *Let the assumptions in Lemmas 2.3-2.4 be satisfied. Then, there exist positive constants $C_5 = C_5(\alpha, k_\mathrm{m}, T)$ such that at time instances $t_{n+1/2} := (t_n + t_{n+1})/2$ we have*

$$\begin{aligned} &\|u^{n+1/2} - u_h^{n+1/2}\| + h|u^{n+1/2} - u_h^{n+1/2}|_1 \\ &\leq C_5\left(|P_h u_0 - u_h^0|_1 + |P_h u(t_1) - u_h^1|_1 + \|D_\tau^+(P_h u_0 - u_h^0)\| + h^{p+1} + \tau^2\right). \end{aligned} \tag{23}$$

Proof. Replacing the FEM by IGA approximation leads to the result by extending [17, 28]. $\square$

3 POD for ROM of parameterized PDEs

ROM of parameterized PDEs aims to reduce the dimension of solution manifolds corresponding to sets of time, physical, and geometric parameters for steady/unsteady problems; specifically, in this paper, we consider the time variable as the unique parameter. POD-Galerkin methods for numerical solutions of PDEs usually demand to first obtain or train a POD basis in which the number of basis functions is expected to be much smaller than that in the full order Galerkin approximation, e.g., FEM. There are two types of POD basis generation approaches [33, 39]: the continuous POD (C-POD) and discrete POD (D-POD), the latter is the approach we consider in this paper.

3.1 D-POD

A continuous and accurate set of snapshots $\{y(t) \,|\, t \in [0, T]\}$ is usually not available in practice, while discrete approximate snapshots can be obtained (as in our case of Eq. (7)) e.g. as follows:

$$\{y_j \,|\, y_j = u_h^{j-1}, j = 1, \ldots, N_t + 1\} \subset X_h. \tag{24}$$

Here, h is the mesh parameter related to spatial IGA discretization, and X_h is a finite-dimensional subspace of X, a Hilbert space typically chosen as $L^2(\Omega)$ or $H^1(\Omega)$. We compute numerical approximations of $y(t)$ by a full discretization method consisting of spatial IGA approximation and Newmark scheme, dicussed in detail in Section 2. Denote $\mathcal{V}_\iota := \text{span}\{y_j \,|\, y_j = u_h^{j-1}, j = 1, \dots, N_t + 1\}$ and $\iota := \dim\mathcal{V}_\iota \le N_t + 1 < \infty$ (in some instances $\iota < N_t + 1$ since in principle snapshots may be linearly dependent). For $r \in \{1, \dots, \iota\}$, the D-POD requires to solve a *finite-dimensional* optimization problem

$$\min_{\{\varphi_k\}_{k=1}^r \subset X_h} \sum_{j=1}^{N_s} \alpha_j \left\| y_j - \sum_{k=1}^r (y_j, \varphi_k)_X \, \varphi_k \right\|_X^2 \tag{25}$$
$$\text{subject to } (\varphi_i, \varphi_j)_X = \delta_{ij} \text{ for } 1 \le i, j \le r$$

to obtain an optimal orthonormal basis $\{\varphi_i\}_{i=1}^r$ of V_r (subspace of $\mathcal{V}_\iota$), where the number of snapshots $N_s = N_t + 1$ at this stage and $\{\alpha_j\}_{j=1}^{N_t+1}$ denote nonnegative weights satisfying $\sum_{j=1}^{N_t+1} \alpha_j = T$. Specifically, we choose trapezoidal weights as in [39], i.e.

$$\alpha_1 = \alpha_{N_t+1} = \frac{\tau}{2} \quad \text{and} \quad \alpha_i = \tau \text{ for } i = 2, \dots, N_t, \tag{26}$$

which ensures that (25) is an approximation of a time integral when τ is small.

3.2 Time derivatives (TD) and time derivative approximations (TDA)

Recently, TD/TDA were suggested to be included in the set of snapshots in analysis of the C-POD/D-POD truncation errors [26, 36]. For D-POD with TDA included, the set of snapshots $\{y_j\}_{j=1}^{N_s}$ with $N_s = 3N_t$ consists of numerical solutions

$$y_j = u_h^{j-1}, \quad j = 1, \dots, N_t + 1$$

plus their TDA counterpart:

$$y_j = D_\tau^+ u_h^{j-N_t-2}, \quad j = N_t + 2, \dots, 2N_t + 1 \tag{27}$$

and

$$y_j = D_\tau^+ D_\tau^- u_h^{j-2N_t-1}, \quad j = 2N_t + 2, \dots, N_s. \tag{28}$$

It is well-known that these TDA can be regarded as second order central difference approximations at $t_{i-1/2} := (i - 1/2)\tau$ for $i = 1, \dots, N_t$. Then, the additional weights $\{\alpha_j\}_{j=N_t+2}^{N_s}$ in problem (25) arising from the TDA, are $\alpha_j = \tau$ for $j = N_t + 2, \dots, N_s$. At this point, we set $\mathcal{V}_\iota \equiv \text{span}\{\bar{\bar{y}}_j\}_{j=1}^\iota$, where $\{\bar{\bar{y}}_j\}_{j=1}^\iota$ denote the linearly independent basis obtained from $\text{span}\{y_j\}_{j=1}^{N_s}$. Notice that the inclusion of TDA approximately triples the cardinality of snapshot-set, but does not change the dimension of the space, which is spanned by snapshots without derivative approximations. As shown in e.g. [19, 26, 25], it is necessary to include TDA for convergence analysis of POD-Galerkin schemes.

We introduce the *correlation matrix*

$$K = [K_{ij}] \in \mathbb{R}^{N_s \times N_s} \quad \text{with} \quad K_{ij} = \frac{1}{N_s}(y_j, y_i)_X, \tag{29}$$

which is symmetric positive semi-definite and has rank ι since $\dim\mathcal{V}_\iota = \iota$. Let $\lambda_1 \ge \dots \ge \lambda_\iota > 0$ denote the nonzero eigenvalues of K and $\lambda_{\iota+1} = \dots = \lambda_{N_s} = 0$ the null ones, then, $v_1, \dots, v_{N_s} \in \mathbb{R}^{N_s}$ are the associated eigenvectors.

Lemma 3.1. *([26]) The POD basis of rank r with $1 \leq r \leq \iota$ (i.e. the solution of problem (25) with/without TDA) is given by*

$$\psi_k = \frac{1}{\sqrt{N_s \lambda_k}} \sum_{j=1}^{N_s} (v_k)_j y_j, \quad k = 1, \dots, r. \tag{30}$$

Moreover, we have the following error formula for the general D-POD from snapshots with or without TDA:

$$\frac{1}{N_s} \sum_{j=1}^{N_s} \|y_j - P_r y_j\|_X^2 = \sum_{k=r+1}^{\iota} \lambda_k, \tag{31}$$

where the projection operator $P_r : V_h \to V_r$ is defined as

$$P_r y_j := \sum_{k=1}^{r} (y_j, \psi_k)_X \psi_k, \quad \forall y_j \in V_h. \tag{32}$$

Specifically, for the TDA-based D-POD, we have different versions of Eq. (31) for different choices of the space X. Let $\widehat{\lambda}_k$ and $\widetilde{\lambda}_k$, $k_m = 1, \dots, \iota$ denote the nonzero eigenvalues of the correlation matrix K with $X = L^2(\Omega)$ and $X = H^1(\Omega)$, respectively. For $X = L^2(\Omega)$, we denote by $\{\widehat{\psi}_k\}_{k=1}^{\iota}$ the POD basis and Eq. (31) implies

$$\frac{1}{3N_t} \sum_{n=0}^{N_t} \left\| u_h^n - \sum_{k=1}^{r} (u_h^n, \widehat{\psi}_k) \widehat{\psi}_k \right\|^2 + \frac{1}{3N_t} \sum_{n=0}^{N_t-1} \left\| D_\tau^+ u_h^n - \sum_{k=1}^{r} (D_\tau^+ u_h^n, \widehat{\psi}_k) \widehat{\psi}_k \right\|^2$$
$$+ \frac{1}{3N_t} \sum_{n=1}^{N_t-1} \left\| D_\tau^+ D_\tau^- u_h^n - \sum_{k=1}^{r} (D_\tau^+ D_\tau^- u_h^n, \widehat{\psi}_k) \widehat{\psi}_k \right\|^2 = \sum_{k=r+1}^{\iota} \widehat{\lambda}_k. \tag{33}$$

For $X = H^1(\Omega)$, we denote by $\{\widetilde{\psi}_k\}_{k=1}^{\iota}$ the POD-basis and Eq. (31) implies

$$\frac{1}{3N_t} \sum_{n=0}^{N_t} \left\| u_h^n - \sum_{k=1}^{r} (u_h^n, \widetilde{\psi}_k)_1 \widetilde{\psi}_k \right\|_1^2 + \frac{1}{3N_t} \sum_{n=0}^{N_t-1} \left\| D_\tau^+ u_h^n - \sum_{k=1}^{r} (D_\tau^+ u_h^n, \widetilde{\psi}_k)_1 \widetilde{\psi}_k \right\|_1^2$$
$$+ \frac{1}{3N_t} \sum_{n=1}^{N_t-1} \left\| D_\tau^+ D_\tau^- u_h^n - \sum_{k=1}^{r} (D_\tau^+ D_\tau^- u_h^n, \widetilde{\psi}_k)_1 \widetilde{\psi}_k \right\|_1^2 = \sum_{k=r+1}^{\iota} \widetilde{\lambda}_k. \tag{34}$$

The POD basis and eigenvalues above for both the cases depend on the discretization parameters h and τ. In the following, if we do not distinguish between the two bases in $L^2(\Omega)$ and $H^1(\Omega)$, we will generally write $\{\psi_i\}_{i=1}^{r}$ and denote by $V_r := \mathrm{span}\{\psi_j\}_{j=1}^{r}$ the *POD space of dimension r* with $V_r \subset \mathcal{V}_\iota$ for $r < \iota$ and $V_r \equiv \mathcal{V}_\iota$ for $r = \iota$. We call V_r *POD space* for simplicity. So far, let us point out that we have introduced the following Hilbert spaces with inclusion relations as:

$$V_r \subseteq \mathcal{V}_\iota \subset V_h \subset V \subseteq H^1(\Omega) \subset L^2(\Omega). \tag{35}$$

Remark 3.2. *Based on snapshots from full discretizations in space and time, POD modes (30) and eigenvalue truncation error (31) differ from those of semi-discretization in time only ([20, 21, 26]), or from those different kind of spatial discretizaton techniques, e.g. FEM ([29]).*

4 IGA-Newmark-POD scheme

The POD basis can be generated by successively using the fully discrete IGA-Newmark method for computing the snapshots and then singular value decomposition of the correlation matrix K for obtaining the POD modes. We then use this basis to derive the POD semi-discrete scheme and POD-Newmark fully discrete scheme.

Given $t \in (0, T]$, the POD-Galerkin semi-discrete scheme consists in finding $u_r(t) \in V_r$ such that

$$\begin{cases} \Big(u_{r,tt}(t), w_r\Big) + a(u_r(t), w_r) = (f(t), w_r) \quad \forall w_r \in V_r \\ u_r(0) = u_{0,r}, \ v_r(0) = v_{0,r}, \end{cases} \tag{36}$$

where $u_{0,r}$ (or $v_{0,r}$) is some projection of $u_{0,h}$ (or $v_{0,h}$) from V_h onto V_r.

Let us define the stiffness matrix $\mathbb{A} = [\mathbb{A}_{ij}] \in \mathbb{R}^{\iota \times \iota}$ with $\mathbb{A}_{ij} := a(\psi_j, \psi_i)$ and mass matrix $\mathbb{M} = [\mathbb{M}_{ij}] \in \mathbb{R}^{\iota \times \iota}$ with $\mathbb{M}_{ij} := (\psi_j, \psi_i)$. Let $\mu_1 \geq \mu_2 \geq \cdots \geq \mu_\iota > 0$ and $\nu_1 \geq \nu_2 \geq \cdots \geq \nu_\iota > 0$ be the eigenvalues of M_ι and singular values of A_ι, respectively; in addition, $\|\cdot\|_2$ denotes the spectral norm of a matrix. Then, we have the following properties in the POD space [41].

Lemma 4.1 (Inequalities in $\mathcal{V}_\iota$). *For all $v \in \mathcal{V}_\iota$, we have*

$$\|v\| \leq \sqrt{\nu_\iota^{-1} \mu_1} \, \|v\|_1 \quad and \quad \|v\|_1 \leq \sqrt{\mu_\iota^{-1} \nu_1} \, \|v\|. \tag{37}$$

with $\nu_1 > \mu_\iota$. In particular,

$$\|v\| \leq \sqrt{\nu_\iota^{-1}} \, \|v\|_1 \quad and \quad \|v\|_1 \leq \sqrt{\nu_1} \|v\| \tag{38}$$

with $\nu_1 > 1$ for POD basis in $X = L^2(\Omega)$ and

$$\|v\| \leq \sqrt{\mu_1} \|v\|_1 \quad and \quad \|v\|_1 \leq \sqrt{\mu_\iota^{-1}} \, \|v\| \tag{39}$$

with $\mu_\iota < 1$ for POD basis in $X = H^1(\Omega)$.

Proof. By Lemma 2 of [26], we have

$$\|v\| \leq \sqrt{\|\mathbb{M}\|_2 \|\mathbb{A}^{-1}\|_2} \|v\|_1 \quad and \quad \|v\|_1 \leq \sqrt{\|\mathbb{A}\|_2 \|\mathbb{M}^{-1}\|_2} \|v\|. \tag{40}$$

By definition of matrix 2-norm, symmetry and positive definite properties of $\mathbb{M}$, $\mathbb{M}^{-1}$, $\mathbb{A}$ and $\mathbb{A}^{-1}$, we easily have

$$\|\mathbb{M}\|_2 = \mu_1, \ \|\mathbb{M}^{-1}\|_2 = \mu_\iota^{-1}, \ \|\mathbb{A}\|_2 = \nu_1, \ and \ \|\mathbb{A}^{-1}\|_2 = \nu_\iota^{-1}. \tag{41}$$

By means of (41) in (40), the inequalities (37), (38), and (39) hold.

By the second inequality of (37) and the fact that $\|v\| \leq \sqrt{1-\alpha} \|v\|_1$ for any $v \in \mathcal{V}_\iota$ from (5), we obtain $(1-\alpha)\nu_1 \geq \mu_\iota$ and thus $\nu_1 > \mu_\iota$ since $\alpha \in (0, 1)$. In particular, for POD basis in $L^2(\Omega)$ or $H^1(\Omega)$, the mass matrix or stiffness matrix turn out to be the identity matrix and so that $\nu_1 > 1$ or $\mu_\iota < 1$ follows. $\square$

Remark 4.2. *The second inequality of (38) (resp. (39)) is an inverse inequality in $\mathcal{V}_\iota$ which is similar (Lemma 2.2) for both the NURBS spaces of IGA and piecewise Lagrange polynomial spaces of FEM (Lemma 3.1 [24]). However, the values of ν_1, ν_ι, μ_1 and μ_ι may significantly differ depending on whether we use IGA or FEM methods.*

Now we present the IGA-Newmark-POD fully discrete scheme: find $u_r^n \in V_r$, $n = 1, \ldots, N_t - 1$ such that

$$\begin{cases} \left(D_\tau^+ D_\tau^- u_r^n, w_r\right) + \frac{1}{2}a\big((u_r^{n-1/2} + u_r^{n+1/2}), w_r\big) = (f^n, w_r) \quad \forall w_r \in V_r, \\ u_r^0 = u_{0,r}, \quad v_r^0 = v_{0,r}, \end{cases} \tag{42}$$

for which we show the following stability property:

Theorem 4.3 (IGA-Newmark-POD Stability). *Assume that $\tau \leq 1$. We have for problem (42) ($n = 1, \ldots, N_t - 1$) the stability estimate:*

$$\|D_\tau^+ u_r^n\|^2 + |u_r^{n+1/2}|_1^2 \leq \mathrm{e}^{2T}\left(\|D_\tau^+ u_r^0\|^2 + |u_r^{1/2}|_1^2 + \sup_{1 \leq k \leq N_t - 1} \|f^k\|^2\right). \tag{43}$$

In the particular case $f = 0$, we obtain the discrete energy conservation principle:

$$\|D_\tau^+ u_r^n\|^2 + |u_r^{n+1/2}|_1^2 = \|D_\tau^+ u_r^0\|^2 + |u_r^{1/2}|_1^2. \tag{44}$$

Proof. We first prove the special case (44) when $f = 0$. Choose $w_r = (u_r^{n+1} - u_r^{n-1})/(2\tau)$ in (42), then

$$w_r = \frac{1}{2}(D_\tau^+ u_r^n + D_\tau^+ u_r^{n-1}) = \frac{1}{\tau}(u_r^{n+1/2} - u_r^{n-1/2}).$$

By this w_r, we have

$$\left(D_\tau^+ D_\tau^- u_r^n, w_r\right) = \frac{1}{2\tau}\left(D_\tau^+ u_r^n - D_\tau^- u_r^n, D_\tau^+ u_r^n + D_\tau^- u_r^n\right) = \frac{1}{2}D_\tau^- \|D_\tau^+ u_r^n\|^2 \tag{45}$$

and

$$\frac{1}{2}a\big((u_r^{n-1/2} + u_r^{n+1/2}), w_r\big) = \frac{1}{2\tau}a\big(u_r^{n-1/2} + u_r^{n+1/2}, u_r^{n-1/2} - u_r^{n+1/2}\big) = \frac{1}{2}D_\tau^- |u_r^{n+1/2}|_1^2.$$

Adding this equation to (45) and setting $f = 0$, we have

$$D_\tau^-\left(\|D_\tau^+ u_r^n\|^2 + |u_r^{n+1/2}|_1^2\right) = 0, \tag{46}$$

from which the result (44) follows.

To prove (43), we have the equality by similar arguments as above

$$D_\tau^-\left(\|D_\tau^+ u_r^n\|^2 + |u_r^{n+1/2}|_1^2\right) = (f^n, D_\tau^+ u_r^n + D_\tau^+ u_r^{n-1}). \tag{47}$$

By Cauchy-Schwarz inequality, we get

$$D_\tau^-\left(\|D_\tau^+ u_r^n\|^2 + |u_r^{n+1/2}|_1^2\right) \leq \|f^n\|^2 + \frac{1}{2}\|D_\tau^+ u_r^n\|^2 + \frac{1}{2}\|D_\tau^+ u_r^{n-1}\|^2. \tag{48}$$

Set $\varsigma_n := \|D_\tau^+ u_r^n\|^2 + |u_r^{n+1/2}|_1^2$, we have

$$\varsigma_n - \varsigma_{n-1} \leq \tau\|f^n\|^2 + \frac{\tau}{2}\varsigma_n + \frac{\tau}{2}\varsigma_{n-1}, \quad n = 1, \ldots, N_t - 1,$$

i.e.,

$$(2 - \tau)\varsigma_n \leq (2 + \tau)\varsigma_{n-1} + 2\tau\|f^n\|^2, \quad n = 1, \ldots, N_t - 1, \tag{49}$$

As $\tau < 1$, we set

$$\beta = \frac{2}{2 - \tau} \sup_{1 \leq k \leq N_t - 1} \|f^k\|^2 \geq 0. \tag{50}$$

11

Then, (49) implies that
$$\varsigma_n \leq \theta\varsigma_{n-1} + \beta\tau$$
with $\theta := (2+\tau)/(2-\tau)$. We have by induction that

$$\varsigma_n \leq \theta^n\varsigma_0 + \beta\tau\sum_{k=0}^{n-1}\theta^k = \theta^n\varsigma_0 + \beta\tau\frac{\theta^n - 1}{\theta - 1}. \tag{51}$$

Since

$$\theta^n = \left(\frac{2+\tau}{2-\tau}\right)^n = \left(1 + \frac{2\tau}{2-\tau}\right)^n \leq e^{\frac{2\tau}{2-\tau}n},$$

(51) implies that

$$\varsigma_n \leq e^{\frac{2\tau}{2-\tau}n}\varsigma_0 + \beta\frac{2-\tau}{2}\left(e^{\frac{2\tau}{2-\tau}n} - 1\right).$$

For $n\tau \leq T$, $n = 0, 1, \ldots, N_t$ and $\tau \leq 1$, thus

$$\varsigma_n \leq e^{2T}\left(\varsigma_0 + \beta\frac{2-\tau}{2}\right). \tag{52}$$

By (52) and the definitions of β and ς_n above, the stability estimate (43) holds. $\qquad\square$

4.1 *A priori* error estimates

We remark that the error bounds of the IGA-Newmark-POD Galerkin scheme include three components arising from IGA space discretization, time discretization and POD eigenvalue truncation.

Theorem 4.4. *Let the assumptions in Lemmas 2.3-2.4 hold. Moreover, we assume $\tau \leq 2\mu_\iota/(\mu_\iota + \nu_1)$. Then, for the IGA-Newmark-POD Galerkin scheme, there exists a constant $C_8 = C_8(\alpha, \beta, \|\nabla\boldsymbol{F}\|_{L^\infty(\widehat{\Omega})}, k_{\mathrm{m}}, \mu_\iota, \nu_1) > 0$ independent of τ, h and p such that*

$$
\begin{aligned}
\frac{1}{N_t}\sum_{n=1}^{N_t-1}\|u^{n+1/2} - u_r^{n+1/2}\|^2 \leq C_8\Big(&|P_hu_0 - u_h^0|_1^2 + |P_hu(t_1) - u_h^1|_1^2 + |P_ru_h^0 - u_r^0|_1^2 + |P_ru_h^1 - u_r^1|_1^2 \\
&+ \|D_\tau^+(P_hu_0 - u_h^0)\|^2 + \|D_\tau^+(P_ru_h^0 - u_r^0)\|^2 + \tau^4 + h^{2p+2} + \sum_{k=r+1}^{\iota}\widehat{\lambda}_k\Big).
\end{aligned}
\tag{53}
$$

Proof. We have by the triangle inequality

$$\|u^{n+1/2} - u_r^{n+1/2}\| \leq \|u^{n+1/2} - u_h^{n+1/2}\| + \|u_h^{n+1/2} - u_r^{n+1/2}\|. \tag{54}$$

The average error related to the first term on right hand side of (54) is bounded via the IGA fully-discrete error estimation in Lemma 2.5:

$$\frac{1}{N_t}\sum_{n=1}^{N_t-1}\|u^{n+1/2} - u_h^{n+1/2}\|^2 \leq 4C_5^2\big(|P_hu_0 - u_h^0|_1^2 + |P_hu(t_1) - u_h^1|_1^2 + \tau^4 + h^{2p+2}\big). \tag{55}$$

To estimate the second term of (54), we write

$$
\begin{aligned}
u_h^{n+1/2} - u_r^{n+1/2} &= (u_h^{n+1/2} - P_ru_h^{n+1/2}) + (P_ru_h^{n+1/2} - u_r^{n+1/2}) \\
&\equiv \eta^{n+1/2} + \rho^{n+1/2}.
\end{aligned}
$$

12

First, we have for $\eta^{n+1/2}$ the average square error

$$\frac{1}{N_t} \sum_{n=0}^{N_t-1} \|\eta^{n+1/2}\|^2 \le \frac{1}{2N_t} \sum_{n=0}^{N_t-1} \|\eta^n\|^2 + \frac{1}{2N_t} \sum_{n=0}^{N_t-1} \|\eta^{n+1}\|^2$$

$$\le \frac{1}{N_t} \sum_{n=0}^{N_t} \|\eta^n\|^2 \le 3 \sum_{i=r+1}^{\iota} \widehat{\lambda}_i,$$

(56)

where we have used Lemma 3.1 in the last inequality.

To estimate $\rho^{n+1/2}$, by (22) and (42), we have for any $w_r \in V_r$:

$$\left(D_\tau^+ D_\tau^- (u_h^n - u_r^n), w_r\right) + \frac{1}{2} a\left((u_h^{n+1/2} + u_h^{n-1/2}) - (u_r^{n+1/2} + u_r^{n-1/2}), w_r\right) = 0.$$

(57)

Then, using (57),

$$(D_\tau^+ D_\tau^- \rho^n, w_r) + \frac{1}{2} a(\rho^{n+1/2} + \rho^{n-1/2}, w_r)$$

$$= (D_\tau^+ D_\tau^- (\rho^n - u_h^n + u_h^n), w_r)$$

$$+ \frac{1}{2} a\left(\rho^{n+1/2} + \rho^{n-1/2} - (u_h^{n+1/2} + u_h^{n-1/2}) + (u_h^{n+1/2} + u_h^{n-1/2}), w_r\right)$$

$$= -(D_\tau^+ D_\tau^- \eta^n, w_r) - \frac{1}{2} a(\eta^{n+1/2} + \eta^{n-1/2}, w_r) \quad \forall w_r \in V_r.$$

(58)

We now apply a superposition principle, splitting $\rho^n = \check{\rho}^n + \bar{\rho}^n$ and $\rho^{n+1/2} = \check{\rho}^{n+1/2} + \bar{\rho}^{n+1/2}$. These quantities are defined to satisfy

$$(D_\tau^+ D_\tau^- \check{\rho}^n, w_r) + \frac{1}{2} a(\check{\rho}^{n+1/2} + \check{\rho}^{n-1/2}, w_r) = 0 \quad \forall w_r \in V_r$$

$$\check{\rho}^0 = \mathcal{P}_r u_h^0 - u_r^0, \quad \check{\rho}^1 = \mathcal{P}_r u_h^1 - u_r^1$$

(59)

and

$$(D_\tau^+ D_\tau^- \bar{\rho}^n, w_r) + \frac{1}{2} a(\bar{\rho}^{n+1/2} + \bar{\rho}^{n-1/2}, w_r) = -(D_\tau^+ D_\tau^- \eta^n, w_r) - \frac{1}{2} a(\eta^{n+1/2} + \eta^{n-1/2}, w_r) \quad \forall w_r \in V_r$$

$$\bar{\rho}^0 = \bar{\rho}^1 = 0,$$

(60)

respectively. We apply Theorem 4.3 to (59) and get

$$\|D_\tau^+ \check{\rho}^n\|^2 + |\check{\rho}^{n+1/2}|_1^2 = \|D_\tau^+ \check{\rho}^0\|^2 + |\check{\rho}^{1/2}|_1^2, \quad n = 1, \ldots, N_t - 1.$$

(61)

The initial condition in (59) allows us to easily have

$$\|D_\tau^+ \check{\rho}^n\|^2 + |\check{\rho}^{n+1/2}|_1^2 \le \frac{1}{2}(|P_r u_h^0 - u_r^0|_1^2 + |P_r u_h^1 - u_r^1|_1^2) + \|D_\tau^+ (P_r u_h^0 - u_r^0)\|^2.$$

(62)

To estimate $\bar{\rho}^n$, we take

$$w_r = \frac{1}{2}(D_\tau^+ \bar{\rho}^n + D_\tau^+ \bar{\rho}^{n-1}) = \frac{1}{\tau}(\bar{\rho}^{n+1/2} - \bar{\rho}^{n-1/2})$$

in (60) and obtain

$$D_\tau^- (\|D_\tau^+ \bar{\rho}^n\|^2 + |\bar{\rho}^{n+1/2}|_1^2)$$

$$= -(D_\tau^+ D_\tau^- \eta^n, D_\tau^+ \bar{\rho}^n) - a(\eta^{n+1/2} + \eta^{n-1/2}, D_\tau^+ \bar{\rho}^n)$$

$$- (D_\tau^+ D_\tau^- \eta^n, D_\tau^+ \bar{\rho}^{n-1}) - a(\eta^{n+1/2} + \eta^{n-1/2}, D_\tau^+ \bar{\rho}^{n-1})$$

$$\le \|D_\tau^+ D_\tau^- \eta^n\| \|D_\tau^+ \bar{\rho}^n\| + \|D_\tau^+ D_\tau^- \eta^n\| \|D_\tau^+ \bar{\rho}^{n-1}\|$$

$$+ \|\eta^{n+1/2} + \eta^{n-1/2}\|_1 \|D_\tau^+ \bar{\rho}^n\|_1 + \|\eta^{n+1/2} + \eta^{n-1/2}\|_1 \|D_\tau^+ \bar{\rho}^{n-1}\|_1$$

13

by the Cauchy-Schwarz inequality and continuity of $a(\cdot,\cdot)$. By using the inverse estimate in Lemma 4.1 in $\mathcal{V}_\iota$ and the Young's type inequality $ab \le a^2 + \frac{1}{4}b^2$, we further have

$$D_\tau^- (\|D_\tau^+ \bar{\rho}^n\|^2 + |\bar{\rho}^{n+1/2}|_1^2) \le 2(\|D_\tau^+ D_\tau^- \eta^n\|^2 + \|\eta^{n+1/2} + \eta^{n-1/2}\|_1^2) \tag{63}$$
$$+ \frac{\mu_\iota + \nu_1}{4\mu_\iota}(\|D_\tau^+ \bar{\rho}^n\|^2 + \|D_\tau^+ \bar{\rho}^{n-1}\|^2).$$

Set $\varsigma_n := \|D_\tau^+ \bar{\rho}^n\|^2 + |\bar{\rho}^{n+1/2}|_1^2$ for $n = 0, 1, \ldots, N_t - 1$. By similar induction arguments as made in Theorem 4.3 showing that (43) from (47), we can obtain from (63) for $n\tau \le T$, $n = 0, 1, \ldots, N_t$ and $\tau \le 2\mu_\iota/(\mu_\iota + \nu_1)$ that

$$\varsigma_n \le e^{\frac{\mu_\iota + \nu_1}{\mu_\iota}T}\left[\varsigma_0 + \beta\frac{4\mu_\iota - (\mu_\iota + \nu_1)\tau}{2(\mu_\iota + \nu_1)}\right], \tag{64}$$

where the number $\beta > 0$ satisfies that

$$\beta\left(1 - \frac{\mu_\iota + \nu_1}{4\mu_\iota}\tau\right) \ge 2(\|D_\tau^+ D_\tau^- \eta^n\|^2 + \|\eta^{n+1/2} + \eta^{n-1/2}\|_1^2).$$

By definitions of ς_n and β, and the fact that $\bar{\rho}^0 = \bar{\rho}^1 = 0$ in (60), we obtain

$$\|D_\tau^+ \bar{\rho}^n\|^2 + |\bar{\rho}^{n+1/2}|_1^2 \le e^{\frac{\mu_\iota + \nu_1}{\mu_\iota}T}\left[\|D_\tau^+ \bar{\rho}^0\|^2 + |\bar{\rho}^{1/2}|_1^2 + \frac{4\mu_\iota}{\mu_\iota + \nu_1}(\|D_\tau^+ D_\tau^- \eta^n\|^2 + \|\eta^{n+1/2} + \eta^{n-1/2}\|_1^2)\right] \tag{65}$$
$$= C_6(\|D_\tau^+ D_\tau^- \eta^n\|^2 + \|\eta^{n+1/2} + \eta^{n-1/2}\|_1^2)$$

with $C_6 = C_6(\mu_\iota, \nu_1, T) := 4\mu_\iota e^{(1+\mu_\iota^{-1}\nu_1)T}/(\mu_\iota + \nu_1)$. A combination of (62) and (65) leads to

$$\|D_\tau^+ \rho^n\|^2 + |\rho^{n+1/2}|_1^2 \le 2(\|D_\tau^+ \breve{\rho}^n\|^2 + |\breve{\rho}^{n+1/2}|_1^2) + 2(\|D_\tau^+ \bar{\rho}^n\|^2 + |\bar{\rho}^{n+1/2}|_1^2)$$
$$\le |P_r u_h^0 - u_r^0|_1^2 + |P_r u_h^1 - u_r^1|_1^2 + 2\|D_\tau^+ (P_r u_h^0 - u_r^0)\|^2$$
$$+ 2C_6(\|D_\tau^+ D_\tau^- \eta^n\|^2 + \|\eta^{n+1/2} + \eta^{n-1/2}\|_1^2),$$

for $n = 1, \ldots, N_t - 1$. Therefore,

$$\frac{1}{N_t}\sum_{n=1}^{N_t-1}|\rho^{n+1/2}|_1^2 \le (|P_r u_h^0 - u_r^0|_1^2 + |P_r u_h^1 - u_r^1|_1^2 + 2\|D_\tau^+ (P_r u_h^0 - u_r^0)\|^2)$$

$$+ \frac{2C_6}{N_t}\sum_{n=1}^{N_t-1}\|D_\tau^+ D_\tau^- \eta^n\|^2 + \frac{2C_6}{N_t}\sum_{n=1}^{N_t-1}\|\eta^{n+1/2} + \eta^{n-1/2}\|_1^2,$$

where by Lemma 3.1

$$\frac{1}{N_t}\sum_{n=1}^{N_t-1}\|D_\tau^+ D_\tau^- \eta^n\|^2 \le 3\sum_{i=r+1}^{\iota}\widehat{\lambda}_i \tag{66}$$

and

$$\frac{1}{N_t}\sum_{n=1}^{N_t-1}\|\eta^{n+1/2} + \eta^{n-1/2}\|_1^2 \le \frac{2}{N_t}\sum_{n=1}^{N_t-1}\frac{1}{4}\|\eta^{n+1}\|_1^2 + \frac{2}{N_t}\sum_{n=1}^{N_t-1}\frac{1}{4}\|\eta^{n-1}\|_1^2 \tag{67}$$
$$\le \frac{1}{N_t}\sum_{n=0}^{N_t}\|\eta^n\|_1^2 \le \frac{1}{N_t}\frac{\nu_1}{\mu_\iota}\sum_{n=0}^{N_t}\|\eta^n\|^2 \le \frac{3\nu_1}{\mu_\iota}\sum_{i=r+1}^{\iota}\widehat{\lambda}_i.$$

Hence, we obtain

$$\frac{1}{N_t}\sum_{n=1}^{N_t-1}|\rho^{n+1/2}|_1^2 \le C_7\left(|P_r u_h^0 - u_r^0|_1^2 + |P_r u_h^1 - u_r^1|_1^2 + \|D_\tau^+ (P_r u_h^0 - u_r^0)\|^2 + \sum_{i=r+1}^{\iota}\widehat{\lambda}_i\right) \tag{68}$$

with $C_7 = C_7(\mu_\iota, \nu_1, T)$. Finally, a combination of (55), (56), (68), (33) and (34) yields the result. □

14

4.2 Numerical linear algebra aspects

The IGA spatial semi-discretized problem (17) is a system of ordinary differential equations. Let us denote by N_x the cardinal number of the multi-index set I, i.e. the number of degrees of freedom of the finite dimensional space V_h. Renumber the index from 1 to N_x for all $\boldsymbol{i} \in I$. By writting $u_h(t) = \sum_{j=1}^{N_x} d_j(t)\mathcal{R}_j$ and $u_{0,h} = \sum_{j=1}^{N_x} d_{0,j}\mathcal{R}_j$ and taking $v_h = \mathcal{R}_i$ $(i = 1, \ldots, N_x)$, problem (17) then turns to

$$\begin{cases} M\ddot{\boldsymbol{d}}(t) + A\boldsymbol{d}(t) = \boldsymbol{f}(t), \ t \in (0, T] \\ \boldsymbol{d}(0) = \boldsymbol{d}_0, \ \dot{\boldsymbol{d}}(0) = \boldsymbol{d}_0', \end{cases} \tag{69}$$

where

$$A = [a_{ij}] \in \mathbb{R}^{N_x \times N_x}, \ a_{ij} = a(R_j, R_i),$$

$$M = [m_{ij}] \in \mathbb{R}^{N_x \times N_x}, \ m_{ij} = \int_\Omega R_j R_i \mathrm{d}x,$$

$$\boldsymbol{d}(t) = (d_1(t), \ldots, d_{N_x}(t))^{\mathrm{T}} \in \mathbb{R}^{N_x}, \ \boldsymbol{d}_0 = (d_{0,1}, \ldots, d_{0,N_x})^{\mathrm{T}} \in \mathbb{R}^{N_x},$$

$$\boldsymbol{f}(t) = (f_1(t), \ldots, f_{N_x}(t))^{\mathrm{T}} \in \mathbb{R}^{N_x}, f_i(t) = \int_\Omega f(t) R_i \mathrm{d}x$$

$$\boldsymbol{d}_0' = (d_{0,1}', \ldots, d_{0,N_x}')^{\mathrm{T}} \in \mathbb{R}^{N_x}$$

with $1 \leq i, j \leq N_x$.

In order to numerically apply a POD algorithm as in Lemma 3.1 [39], we require to introduce a weighted inner product in $\mathbb{R}^{N_x}$ for the IGA control variables to replace the inner products in the finite-dimensional (N_x-dimensional) space V_h. The induced norms are also changed accordingly. Let us consider two arbitrary vectors $\boldsymbol{a}, \boldsymbol{b} \in \mathbb{R}^{N_x}$, with $\boldsymbol{a} = (a_i)_{1 \leq i \leq N_x}$ and $\boldsymbol{b} = (b_i)_{1 \leq i \leq N_x}$, then we define the weighted inner product $\langle \cdot, \cdot \rangle_W$ in $\mathbb{R}^{N_x}$ as

$$\langle \boldsymbol{a}, \boldsymbol{b} \rangle_W := \boldsymbol{a}^{\mathrm{T}} W \boldsymbol{b} = \sum_{i=1}^{N_x} \sum_{j=1}^{N_x} a_i W_{ij} b_j, \tag{70}$$

where $W = [w_{ij}]_{1 \leq i,j \leq N_x} \in \mathbb{R}^{N_x \times N_x}$ denotes a symmetric positive definite weight matrix. We then denote the induced norm $|\cdot|_W := \langle \cdot, \cdot \rangle^{1/2}$. Then, $\forall v_h, w_h \in V_h$, since $v_h(x) = \sum_{i=1}^{N_x} a_i \mathcal{R}_i(x)$ and $w_h(x) = \sum_{i=1}^{N_x} b_i \mathcal{R}_i(x)$ are elements of the finite-dimensional subspace $V_h \subset \mathbb{R}^{N_x}$ of V, we have $(v_h, w_h) = \langle \boldsymbol{a}, \boldsymbol{b} \rangle_W$ and $\|v_h\| = |\boldsymbol{a}|_W$ with $W = M$. Analogously, we obtain $(v_h, w_h)_V = \langle \boldsymbol{a}, \boldsymbol{b} \rangle_W$ and $\|u_h\|_1 = |\boldsymbol{a}|_W$ with $W = M + A$.

The algebraic form of (22) reads: find $\{\boldsymbol{d}_h^n\}_{n=1}^{N_t} \subset V_h$ such that

$$\begin{cases} MD_\tau^+ D_\tau^- \boldsymbol{d}_h^n + \dfrac{1}{2} A(\boldsymbol{d}_h^{n+1/2} + \boldsymbol{d}_h^{n-1/2}) = \boldsymbol{f}^n, \quad n = 0, \ldots, N_t - 1, \\ \boldsymbol{d}_h^0 = \boldsymbol{d}_{0,h}, \end{cases} \tag{71}$$

where $\boldsymbol{d}^n = [\boldsymbol{d}_1^n, \ldots, \boldsymbol{d}_{N_x}^n]^{\mathrm{T}}$ for $n = 0, 1, \ldots, N_t$.

We can define a matrix-vector form for the Galerkin POD semi-discretization:

$$\begin{cases} M_r \ddot{\boldsymbol{d}}_r(t) + A_r \boldsymbol{d}_r(t) = \boldsymbol{f}_r(t), \quad t \in (0, T], \\ \boldsymbol{d}_r(0) = \boldsymbol{d}_{r,0} \end{cases} \tag{72}$$

where

$$A_r = [a_{r,ij}] \in \mathbb{R}^{r \times r}, a_{r,ij} := a(\psi_j, \psi_i), \quad M_r = [m_{r,ij}] \in \mathbb{R}^{r \times r}, m_{r,ij} := \int_\Omega \psi_j \psi_i \mathrm{d}x,$$

$$\boldsymbol{d}_r(t) = (d_{r,1}(t), \ldots, d_{r,r}(t))^{\mathrm{T}} \in \mathbb{R}^r, \ \boldsymbol{d}_{r,0} = (d_{0r,1}, \ldots, d_{0r,r})^{\mathrm{T}} \in \mathbb{R}^r,$$

$$\boldsymbol{f}_r(t) = (f_{r,1}(t), \ldots, f_{r,r}(t))^{\mathrm{T}} \in \mathbb{R}^r, \ f_{r,i}(t) := \int_\Omega f(t)\psi_i \mathrm{d}x$$

15

with $1 \leq i, j \leq r$.

The matrix-vector form for IGA-Newmark-POD scheme reads:

$$\begin{cases} M_r D_\tau^+ D_\tau^- \boldsymbol{d}_r^n + \dfrac{1}{2} A_r (\boldsymbol{d}_r^{n+1/2} + \boldsymbol{d}_r^{n-1/2}) = \boldsymbol{f}_r^n, \quad n = 0, \ldots, N_t - 1 \\ \boldsymbol{d}_r^0 = \boldsymbol{d}_{r,0}. \end{cases} \tag{73}$$

By solving this system, we obtain $\{\boldsymbol{d}_r^n\}_{n=0}^{N_t}$ which leads to the POD Galerkin solution $\{u_r^n\}_{n=0}^{N_t}$ with $u_r^n = \sum_{j=1}^r d_{r,j}^n \psi_j$. The POD mass matrix M_r, POD-stiffness matrix A_r, the inverse matrices M_r^{-1} and A_r^{-1} are positive definite [26, 24].

4.3   Algorithm

We present the whole IGA-POD Galerkin methodology for ROM in the form of `Algorithm` 1 which contains three modules: the snapshot computation by IGA, the POD-basis generation and the POD Galerkin approach. Let us denote a diagonal matrix $\Theta = \mathrm{diag}(\alpha_1, \ldots, \alpha_{N_s})$. In `Algorithm` 1, we consider three approaches to generate POD basis as suggested in [39]. These are mathematically equivalent for modal analysis, although their computational costs are generally different from each other. The correlation matrix (29) and POD-basis (31) correspond to Case 3.

The choice of POD rank r is crucial since it influences the accuracy of the POD ROM in approximating the original problem. In our IGA-POD method, we can determine it also based on a heuristic rule [39]. More precisely, given an error tolerance ϵ ($0 < \epsilon \ll 1$), we determine r such that the computed energy ratio

$$E(r) := \frac{\sum_{i=1}^r \lambda_i}{\sum_{i=1}^\iota \lambda_i} > 1 - \epsilon, \tag{74}$$

or equivalently,

$$1 - E(r) = \frac{\sum_{i=r+1}^\iota \lambda_i}{\mathrm{trace}(D^\mathrm{T} D)} < \epsilon \tag{75}$$

with D defined in `Algorithm` 1.

The time and space discretizations have direct effect on the correlation matrix and thus on its eigenvalues. More precisely, the parameters τ, p, k_m and h influence the accuracy of $\{\lambda_i\}_{i=1}^d$. Moreover, the choice of weight W (i.e. $W = M$ or $W = M + A$ for $X = L^2(\Omega)$ or $H^1(\Omega)$, respectively) and the inclusion of TDA (i.e. $N_s = 3N_t$ or $N_s = N_t + 1$) can also affect the eigenvalue analysis. Once the eigenvalues have been computed however, we find from (75) that the POD rank r only directly depends on ϵ. The smaller is ϵ, the larger is r, which leads to more accurate POD Galerkin approximations to snapshots.

Once the POD rank and POD-basis have been determined, we set

$$\Psi = [\psi_1 | \ldots | \psi_r] \in \mathbb{R}^{N_x \times r}.$$

Then, we obtain for (73):

$$M_r = \Psi^\mathrm{T} M \Psi, \quad A_r = \Psi^\mathrm{T} A \Psi, \quad \boldsymbol{f}_r^n = \Psi^\mathrm{T} \boldsymbol{f}^n \text{ for } n = 1, \ldots, N_t.$$

We compute $\boldsymbol{d}_r^n$ by solving (73) and obtain $u_r^n = \Psi \boldsymbol{d}_r^n$.

5   Numerical examples

We use the IGA library `GeoPDEs` [16] to perform numerical simulation in MATLAB. We then assume that the error due to time discretization is relatively "small" compared with the two error components due to space

---

Algorithm 1 IGA-Newmark-POD method for ROM of acoustic wave equations
---
1: **procedure** SNAPSHOTS (Method of snapshots based on IGA-Newmark-scheme)
2: **Require:** Set τ, $N_s = 3[T/\tau]$ (or $([T/\tau]+1)$ if TDA are included or not), p, k_{m}, N_x, and ϵ;
3:      Solve acoustic wave equation by IGA-Newmark scheme to obtain snapshots $\{\boldsymbol{d}_h^n\}_{n=0}^{N_s} \subset \mathbb{R}^{N_x}$;
4: **return** $D = \left[\boldsymbol{d}_h^1 | \ldots | \boldsymbol{d}_h^{N_s}\right] \in \mathbb{R}^{N_x \times N_s}$;

5: **procedure** POD (POD-basis of rank r)
6: **Require:** Weight matrix W, diagonal matrix Θ for temporal quadrature weights;
7: Case 1: if $N_x = N_s$
8:      Compute $\bar{D} = W^{1/2} D \Theta^{1/2}$;
9:      Perform the singular value decomposition: $\bar{D} = \bar{\Psi} \Sigma \bar{\Phi}^{\mathrm{T}}$;
10:      Determine POD rank r;
11:      Compute $\psi_i = W^{-1/2} \bar{\Psi}(:,i) \in \mathbb{R}^{N_x}$ and set $\lambda_i = \Sigma_{ii}^2$ for $i = 1, \ldots, r$;
12: Case 2: if $N_x < N_s$
13:      Compute $\bar{D} = W^{1/2} D \Theta^{1/2}$;
14:      Compute $R = \bar{D} \bar{D}^{\mathrm{T}} \in \mathbb{R}^{N_x \times N_x}$;
15:      Perform the eigenvalue decomposition: $R = \bar{\Psi} \Lambda \bar{\Psi}^{\mathrm{T}}$;
16:      Determine POD rank r;
17:      Compute $\psi_i = W^{-1/2} \bar{\Psi}(:,i) \in \mathbb{R}^{N_x}$ and set $\lambda_i = \Lambda_{ii}$ for $i = 1, \ldots, r$;
18: Case 3: if $N_x > N_s$
19:      Compute $K = \Theta^{1/2} D^{\mathrm{T}} W D \Theta^{1/2} \in \mathbb{R}^{N_s \times N_s}$;
20:      Perform the eigenvalue decomposition: $K = \bar{\Phi} \Lambda \bar{\Phi}^{\mathrm{T}}$;
21:      Determine POD rank r;
22:      Compute $\psi_i = D \Theta^{1/2} \bar{\Phi}(:,i)/\sqrt{\lambda_i} \in \mathbb{R}^{N_x}$ and set $\lambda_i = \Lambda_{ii}$ for $i = 1, \ldots, r$;
23: **return** IGA-POD-basis $\{\psi_i\}_{i=1}^r$ and eigenvalues $\{\lambda_i^h\}_{i=1}^r$.

24: **procedure** POD GALERKIN SCHEME (MOR)
25: **Require:**
26:      Solve PDE by the full discrete POD-Newmark-scheme to obtain POD-basis coefficients $\{\boldsymbol{d}_r^n\}_{n=0}^{N_t} \subset \mathbb{R}^r$;
27:      Compute $u_r^n = \sum_{j=1}^r (\boldsymbol{d}_r^n)_j \psi_j$ for $n = 0, \ldots, N_t$;
28: **return** POD Galerkin solutions $\{u_r^n\}_{n=0}^{N_t}$.
---

discretization and POD projection, i.e. $\tau^2 \ll h^{p+1}$ (or h^p) for L^2-norm (or H^1-norm) and $\tau^2 \ll \sqrt{\epsilon}$. The spatial discretization is carried out by means of NURBS-based IGA with piecewise B-splines or NURBS of different degrees and smoothness. For the generation of the POD basis, we consider the choices of $X = H^1(\Omega)$ (or $L^2(\Omega)$) and possible including TDA. Let us first introduce some notations. The discrete average norms of total error, snapshot error and POD error in (1) are denoted by

$$\mathcal{E}_b := \sqrt{\frac{1}{N_t} \sum_{n=0}^{N_t-1} \|u^{n+1/2} - u_r^{n+1/2}\|_b^2},$$

$$\mathcal{E}_b^h := \sqrt{\frac{1}{N_t} \sum_{n=0}^{N_t-1} \|u^{n+1/2} - u_h^{n+1/2}\|_b^2} \quad \text{and} \quad \mathcal{E}_b^r := \sqrt{\frac{1}{N_t} \sum_{n=0}^{N_t-1} \|u_h^{n+1/2} - u_r^{n+1/2}\|_b^2},$$

respectively, where b denotes $L^2(\Omega)$ (or $H^1(\Omega)$). By using Theorem 4.4 and (74), the expected error bound $\mathcal{E}_{L^2}$ (resp. $\mathcal{E}_{H^1}$) should behave $\mathcal{O}(\tau^2 + h^{p+1} + \sqrt{\epsilon})$ (resp. $\mathcal{O}(\tau^2 + h^p + \sqrt{\epsilon})$).

Example 5.1. Consider an annular domain $\Omega = \{(\rho, \theta)|1 < \rho < 2, 0 < \theta < \pi/2\}$. We set $T = 1$ and

$\tau = 10^{-3}$, for which $\mathcal{O}(\tau^2) = \mathcal{O}(10^{-6})$. Choose as exact solution

$$u(x, y, t) = e^{-\frac{t}{2}} \sin\left(\pi t \left(2x^2 - xy + y^2 - 3x + y\right)\right),$$

and impose Neumann boundary conditions on two arches and Dirichlet boundary conditions on straight lines $\Gamma_D = \partial\Omega \setminus \Gamma_N$. In Fig. 1, we show that triangular mesh required by standard FEM causes geometric modelling errors, while exact representation of Ω can be achieved by NURBS-based geometric modelling in IGA. We show an IGA-POD Galerkin solution at final time.

First, we check the convergence order for errors of snapshots with respect to mesh and time parameters. For meshes used in IGA, we initialize the number of mesh elements as $4 \times 8 = 32$. NURBS allows an exact representation of Ω already at the coarsest level of discretization. We then use h-refinement three times up to an element number $32 \times 64 = 2048$. Fig. 2 shows that the convergence rates for errors of snapshots $\mathcal{E}_b^h$ by IGA $p = 2$ NURBS basis functions with $k_{\mathrm{m}} = 0$ or 1 in both L^2 and H^1 norms, i.e. they are optimal with respect to NURBS-based spatial discretization.

We use three different levels of number of degrees of freedom (ndofs) for comparison. Denote by IGA_0 and IGA_1 be IGA of $p = 2$ with $k_{\mathrm{m}} = 0$ and $k_{\mathrm{m}} = 1$, respectively. As in [41], numerical comparisons in Table 1 shows that the truth approximations by IGA are more accurate than those by FEM, even if less ndofs are used. Moreover, the numerical solutions for the IGA case $k_{\mathrm{m}} = 1$ are more accurate than those for $k_{\mathrm{m}} = 0$ though slightly less ndofs are used. In Fig. 3, different truth approximations may lead to different decay behaviors for the first few POD eigenvalues. If no TDA are included in snapshots, it shows that the three cases visually have nearly the same POD eigenvalues. For the TDA included case, however, both IGA-based cases decay faster than FEM-based case and the IGA_1 case decays faster than the IGA_0 case. This shows that the POD rank r of either the two IGA cases is nearly the same as that of the FEM case if no TDA included. For the TDA included case, however, the POD ranks of the two IGA cases are smaller than that of FEM and the value r of IGA_1 is smaller than that of IGA_0. Since smaller r means more efficient POD-Galerkin methods for ROM, the IGA_1 case is the most efficient and the FEM case is the slowest among three candidates for ROM. We also see that the values eigenvalues are increased if TDA are included. From both Table 2 and Table 3 with a same ϵ, total errors of POD IGA_1 are most accurate and POD IGA_0 is also more accurate than FEM. We also see in Table 3 that the IGA_1 case is the most efficient one for POD-based ROM according to values of r. IGA_0 case is also efficient than FEM.

Table 1: Comparisons on errors of truth approximations for Example 5.1.

N_x			$\mathcal{E}_{L^2}^h$			$\mathcal{E}_{H^1}^h$		
FEM	IGA_0	IGA_1	FEM	IGA_0	IGA_1	FEM	IGA_0	IGA_1
369	341	336	1.58e-2	1.05e-2	3.03e-3	5.84e-1	4.54e-1	1.61e-1
1347	1275	1248	2.21e-3	1.47e-3	2.66e-4	1.69e-1	1.19e-1	3.53e-2
5007	4851	4800	3.35e-4	2.06e-4	4.26e-5	5.00e-2	3.17e-2	8.80e-3

Example 5.2. In this case, we show the advantage of smoothness of B-splines basis functions over FEM with C^0-continuous without any geometric approximation. We set Ω to be a unit square $(0, 1)^2$ and set

(a) Triangular mesh in FEM   (b) Control points (red)   (c) NURBS based mesh

(d) IGA-POD solution at $T = 1$ with 48×96 mesh elements, $p = 2, k_m = 1, \epsilon = 10^{-8}$ (e) Absolute error $|u^{N_t} - u_r^{N_t}|$ (f) Computed first POD mode
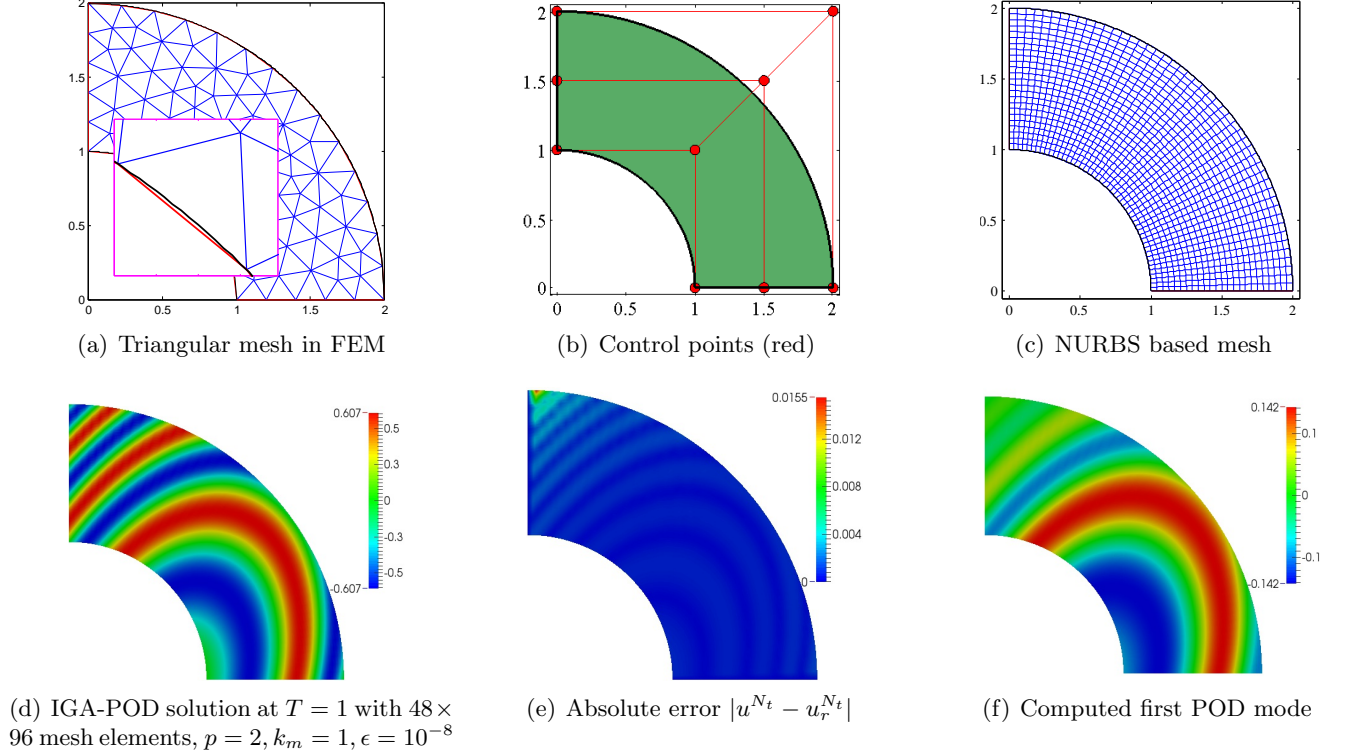
Figure 1: Triangulartion, control points, NURBS based mesh, POD Galerkin solution, its error distribution and the first computed POD mode for Example 5.1.

Table 2: Comparisons on total errors $\mathcal{E}_b$ of POD solutions for Example 5.1: without TDA, $\epsilon = 10^{-6}$.

N_x			X	$\mathcal{E}_{L^2}$			$\mathcal{E}_{H^1}$		
FEM	IGA_0	IGA_1		FEM	IGA_0	IGA_1	FEM	IGA_0	IGA_1
1347	1275	1248	H^1	2.21e-3	1.47e-3	2.66e-4	1.69e-1	1.19e-1	3.53e-2
			L^2	2.22e-3	1.47e-3	3.43e-4	1.69e-1	1.19e-1	3.65e-2
5007	4851	4800	H^1	3.35e-4	2.06e-4	4.16e-5	5.00e-2	3.17e-2	8.61e-3
			L^2	4.40e-4	3.01e-4	2.18e-4	5.21e-2	3.30e-2	1.61e-2

$T = 1$ and $\tau = 10^{-3}$. We choose as exact solution

$$u(x, y, t) = \frac{1}{25} \sum_{j=1}^{5} \sum_{i=1}^{5} \sin(i\pi x) \sin(j\pi y) \cos(\sqrt{i^2 + j^2}\pi t),$$

which satisfies homogeneous Dirichlet boundary conditions. We consider the degree of B-spline basis functions $p = 2, 3$, and 4 with $k_m \geq 1$.

    Both square elements-based IGA and FEM allow an exact geometric representation. Considering that C^0-continuous ($k_m = 0$) B-splines still remain not interpolatory, IGA method in this case is different from the Lagrange basis functions-based FEM for $p \geq 2$. In Fig. 4, we show a POD Galerkin solution. For the same degree p in Table 4, the accuracy of truth approximation is enhanced by increasing the smoothness although less ndofs are used. We see from Table 5 that k-refinement performed by increasing p and k_m simultaneously can increase the accuracy of truth approximation and so that the accuracy of the final POD soultion at a cost of slightly more ndofs used. For both cases, with and without TDA, we find from Fig. 5
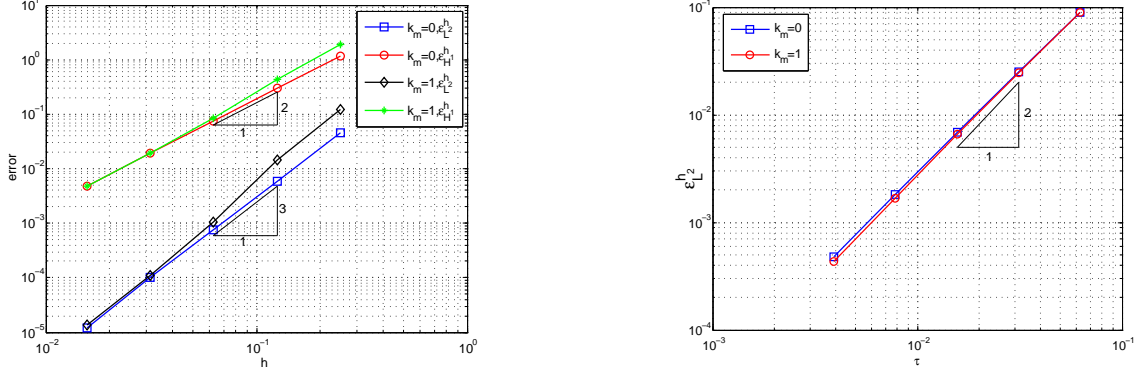
Figure 2: Convergence rate of IGA truth approximations w.r.t. h (left) and τ (right) for Example 5.1: $p = 2$.

Table 3: Comparisons on total errors of POD solutions $\mathcal{E}_b$ for Example 5.1: TDA included, $\epsilon = 10^{-6}$.

X	r			$\mathcal{E}_{L^2}$			$\mathcal{E}_{H^1}$		
	FEM	IGA$_0$	IGA$_1$	FEM	IGA$_0$	IGA$_1$	FEM	IGA$_0$	IGA$_1$
N_x : 1347 (FEM), 1275 (IGA$_0$), 1248 (IGA$_1$)									
H^1	43	38	30	2.22e-3	1.48e-3	3.28e-4	1.69e-1	1.19e-1	3.61e-2
L^2	24	10	10	2.25e-3	1.52e-3	5.44e-4	1.71e-1	1.22e-1	4.65e-2
N_x: 5007 (FEM), 4851 (IGA$_0$), 4800 (IGA$_1$)									
H^1	104	83	69	3.57e-4	2.59e-4	1.68e-4	5.03e-2	3.24e-2	1.06e-2
L^2	64	63	52	5.34e-4	4.97e-4	4.68e-4	5.86e-2	4.57e-2	3.16e-2

that POD eigenvalues decay very fast; POD eigenvalues with $X = L^2$ are smaller in magnitude than those with $X = H^1$. POD eigenvalues of TDA case are larger than those of no TDA case.

Table 4: Errors of truth approximations $\mathcal{E}_b^h$ by smoothness of basis functions for Example 5.2.

p	k_m	N_x	$\mathcal{E}_{L^2}^h$	$\mathcal{E}_{H^1}^h$
2	0	961	3.39e-4	3.12e-2
	1	400	1.78e-4	1.99e-2
3	0	2209	2.17e-5	2.76e-3
	1	1600	2.03e-5	2.01e-3
	2	676	1.69e-5	1.23e-3
4	0	3969	1.538e-5	3.30e-4
	1	3600	1.537e-5	3.05e-3
	2	2601	1.534e-5	2.98e-4
	3	1156	1.532e-5	2.95e-4

Example 5.3. We employ both advantages of IGA shown in examples before: exact representation of geometric domain by NURBS and smoothness of B-spline basis functions to enhance accuracy and efficiency
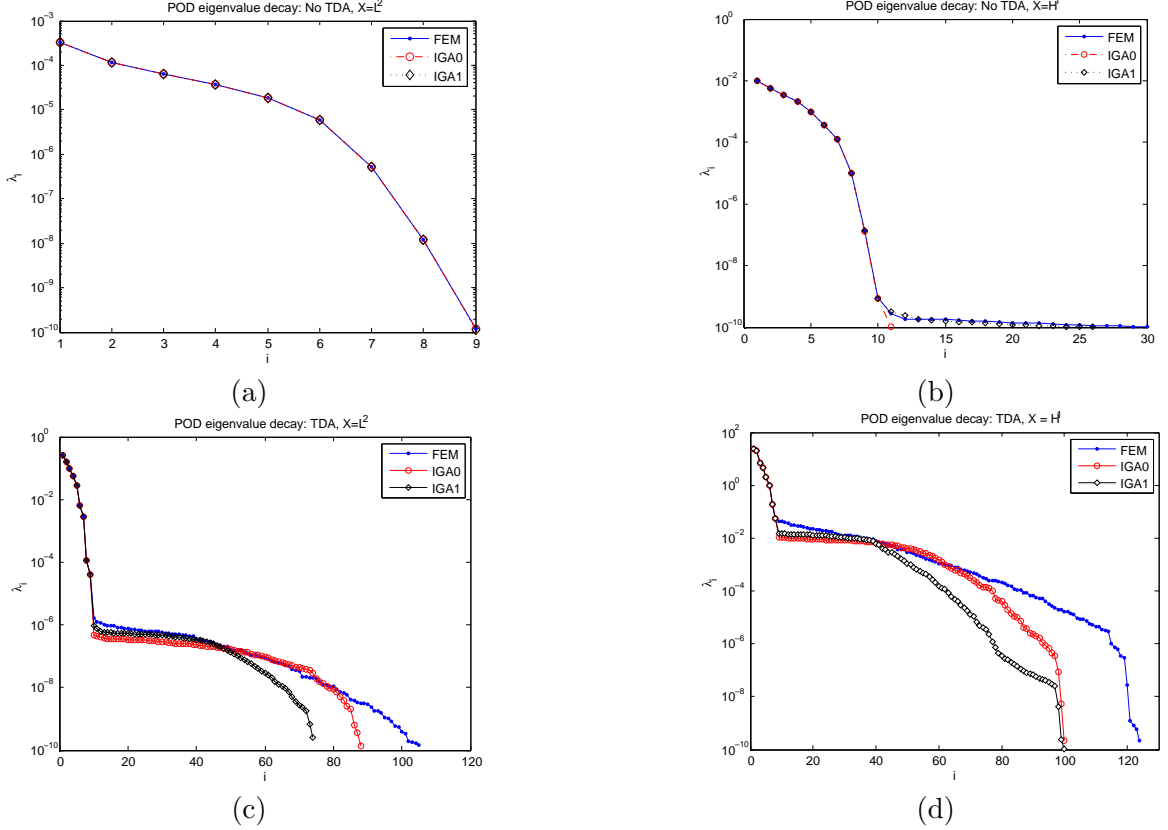
Figure 3: Decay of first few POD eigenvalues (i: index) obtained for $X = L^2(\Omega)$ (left) or $X = H^1(\Omega)$ (right) and without TDA (top) or with TDA (bottom) for Example 5.1: $\epsilon = 10^{-6}$, $N_x = 5007$, 4851 and 4800 for FEM, IGA$_0$ and IGA$_1$, respectively.

in POD model order reduction. Consider a wave propagation problem in a three dimensional quarter of cylindrical annulus $\Omega = (1, 2) \times (0, \pi/2) \times (0, 1)$ in cylindrical coordinates. Set exact solution as

$$u(x, y, z, t) = \begin{cases} e^{-\pi^2 \left(t - \frac{1}{2}(x + y + \sqrt{2}z - 1) - 1\right)^2}, & t \geq \frac{1}{2}(x + y + \sqrt{2}z - 1) \\ 0 & \text{otherwise} \end{cases}$$

satisfying Neumann boundary conditions on $\partial\Omega$. Set $T = 1.5$, $\tau = 2.5 \times 10^{-3}$. Choose $p = 3, k_m = 2$ and set 16, 32 and 16 as number of elements in direction x, y and z, respectively. See Fig. 6 a NURBS based mesh and a POD Galerkin solution with $p = 3, k_m = 2$ and $N_x = 11016$. The computed error of truth approximation is $\mathcal{E}^h_{L^2}$ =5.68e-5. Fig. 7 shows the first few POD eigenvalues with $X = H^1$. In Table 6, we show that the reduced order r increases as ϵ decreases. Thus, the POD truncation error decreases and the final POD solution becomes more accurate.

Table 5: Results by k-refinement for Example 5.2: No TDA, $h = 1/32, \epsilon = 10^{-6}, X = H^1, r = 10$.

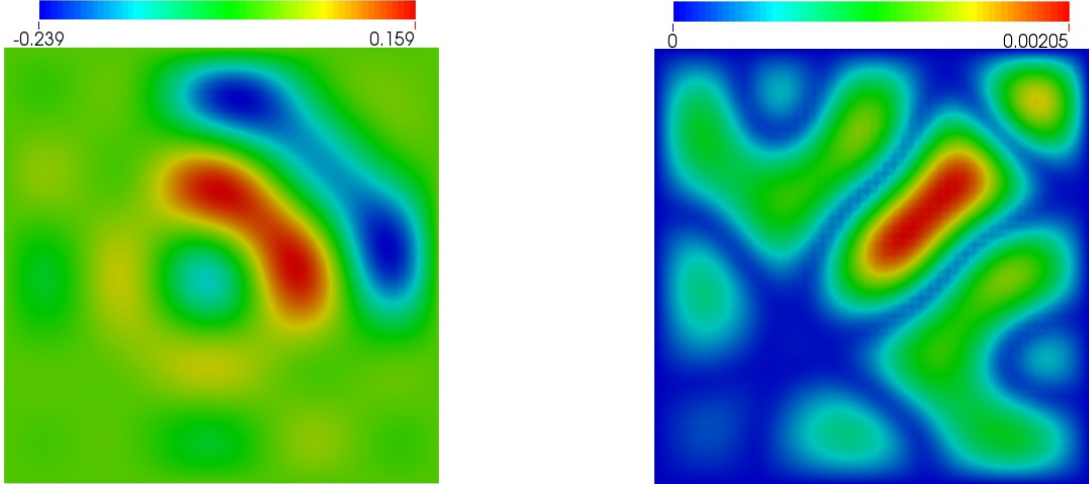| p	k_m	N_x	$\mathcal{E}^h_{L^2}$	$\mathcal{E}^h_{H^1}$	$\mathcal{E}_{L^2}$	$\mathcal{E}_{H^1}$
1	0	961	4.47e-3	1.50e-1	4.47e-3	1.50e-1
2	1	1024	3.20e-5	7.45e-3	3.26e-5	7.45e-3
3	2	1089	1.55e-5	6.25e-4	1.68e-5	6.31e-4
4	3	1156	1.53e-5	2.95e-4	1.66e-5	3.09e-4

21

Figure 4: POD solution at final time (Left) and absolute error $|u^{N_t} - u_r^{N_t}|$ (Right): $h = 1/32, p = 4, k_m = 3, \epsilon = 10^{-8}$.

Table 6: Results w.r.t. ϵ for Example 5.3: $X = H^1$.

ϵ	No TDA			TDA		
	r	$\mathcal{E}^r_{L^2}$	$\mathcal{E}_{L^2}$	r	$\mathcal{E}^r_{L^2}$	$\mathcal{E}_{L^2}$
10^{-3}	4	2.60e-3	1.30e-3	5	1.05e-2	5.28e-3
10^{-4}	5	5.31e-4	2.70e-4	10	6.06e-4	3.06e-4
10^{-5}	6	1.01e-4	7.63e-5	39	1.62e-4	1.00e-4
10^{-6}	6	1.01e-4	7.63e-5	54	4.61e-5	6.12e-5
10^{-7}	7	1.99e-5	5.76e-5	173	6.36e-6	5.71e-5

6   Conclusions

We used IGA in POD for ROM of acoustic wave equations, which may be thought of as one dimensional parameterized model in ROM with the time being the only parameter. We split the error of the POD-Galerkin solution into two parts and show both the accuracy of truth approximation and POD truncation are important for obtaining accuracy and efficiency of POD-Galerkin methods. We discretize the model by IGA and the Newmark scheme and propose a fully IGA-Newmark-POD Galerkin scheme. We analyze the stability and convergence of the discrete schemes by *a priori* error estimates. Numerical experiments are performed, which show promising advantages of IGA for accuracy and efficiency in ROM both with respect to the "exact" geometrical representation of computational domains of practical interest and the use of smooth basis functions allowed by NURBS.

References

[1] R. Abgrall and D. Amsallem, Robust model reduction by L-norm minimization and approximation via dictionaries: application to linear and nonlinear hyperbolic problems, submitted, 2015.
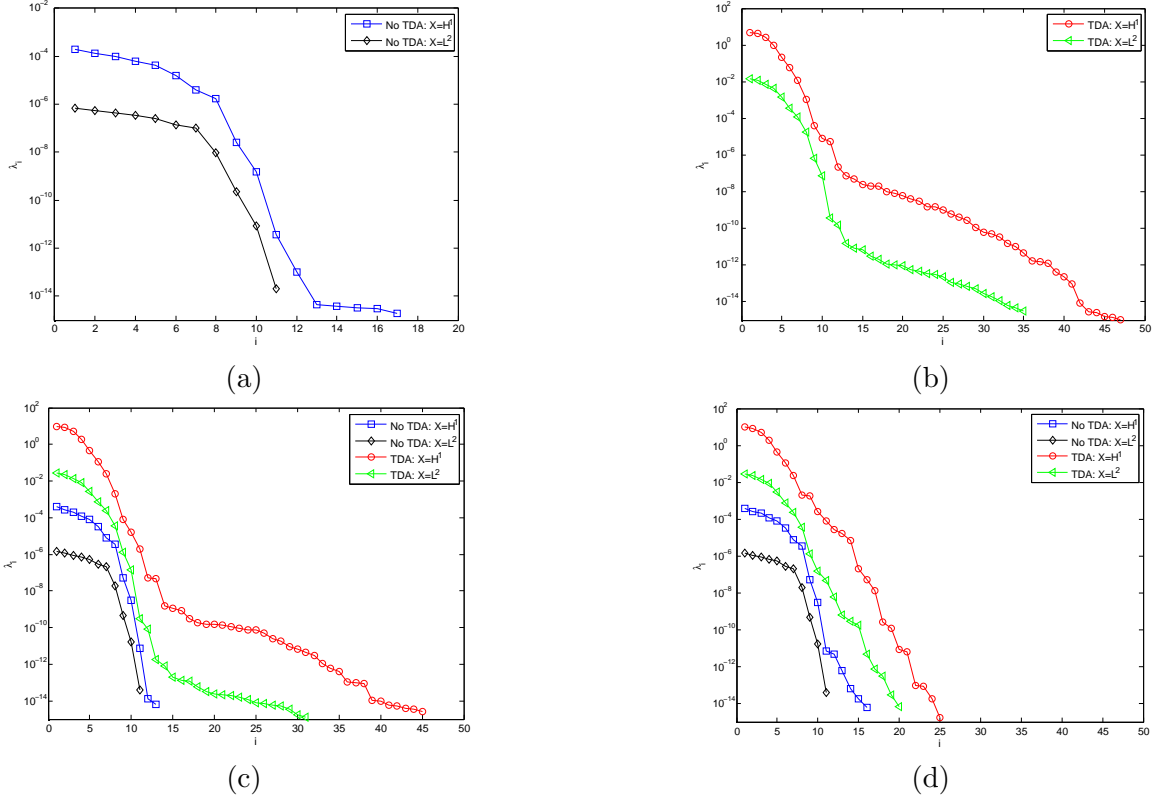
Figure 5: Decay of first few eigenvalues of correlation matrix obtained in $X = L^2/H^1$ and with/without TDQ for Example 5.2 ($h = 1/32$): (a) $p = 3$, $k_m = 2$, $N_x = 1225$ (No TDA); (b) $p = 3$, $k_m = 2$, $N_x = 1225$ (TDA); (c) $p = 4$, $k_m = 3$, $N_x = 1296$; (d) $p = 3$, $k_m = 1$, $N_x = 4356$.

[2] D. Amsallem and U. Hetmaniuk, Error estimates for Galerkin reduced-order models of the semi-discrete wave equation. *ESAIM: M2AN* 48 (2014) 135-163.

[3] A. Bartezzaghi, L. Dedè and A. Quarteroni, Isogeometric analysis of high order partial differential equations on surfaces. *Comput. Methods Appl. Mech. Engrg.* 295 (2015) 446-469.

[4] Y. Bazilevs, L. Beirão de Veiga, J.A. Cottrell, T.J.R. Hughes and G. Sangalli, Isogeometric analysis: approximation, stability and error estimates for *h*-refined meshes. *Math. Models Methods Appl. Sci.* 16 (2006) 1031-1090.

[5] L. Beirão de Veiga, A. Buffa, J. Rivas and G. Sangalli, Some estimates for *h-p-k*-refinement in isogeometric analysis. *Numer. Math.* 118 (2011) 271-305.

[6] G. Berkooz, P. Holmes and J.L. Lumley, The proper orthogonal decomposition in the analysis of turbulent flows. *Annu. Rev. Fluid Mech.* 25 (1993) 539-575.

[7] A. Buffa, G. Sangalli and R. Vázquez, Isogeometric analysis in electromagnetics: B-splines approximation. *J. Comput. Phys.* 199 (2010) 1143-1152.

[8] D. Chapelle, A. Gariah and J. Sainte-Marie, Galerkin approximation with proper orthogonal decomposition: new error estimates and illustrative examples. *ESAIM: M2AN* 46 (2012) 731-757.

[9] J.A. Cottrell, T.J.R. Hughes and Y. Bazilevs, *Isogeometric Analysis: Toward Integration of CAD and FEA.* John Wiley & Sons, 2009.
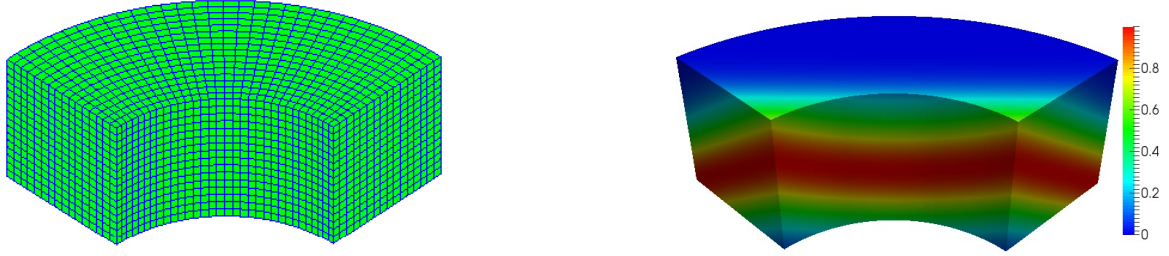
Figure 6: NURBS based mesh and POD solution for Example 5.3 at $T = 1.5$ with $p = 3, k_m = 2, N_x = 11016, \epsilon = 10^{-8}$.
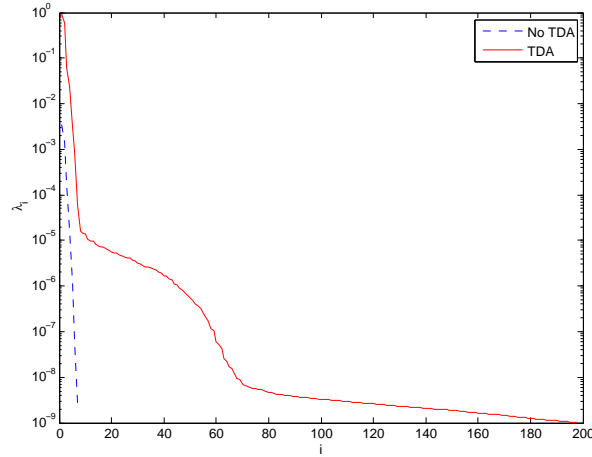

Figure 7: POD eigenvalues for Example 5.3 with $X = H^1$.

[10] J.A. Cottrell, T.J.R. Hughes and A. Reali, Studies of refinement and continuity in Isogeometric structural analysis. *Comput. Methods Appl. Mech. Engrg.* 196 (2007) 4160-4183.

[11] W. Dahmen, C. Plesken and G. Welper, Double greedy algorithms: reduced basis methods for transport dominated problems. *ESAIM: M2AN.* 48 (2014) 623-663.

[12] R. Dautray and J.L. Lions, *Mathematical Analysis and Numerical Methods for Science and Technology, in Evolution Problems I*, vol. 5, II, vol. 6, Springer-Verlag, Berlin, 1992.

[13] L. Dedè, M.J. Borden and T.J.R. Hughes, Isogeometric analysis for topology optimization with a phase field model. *Arch. Comput. Methods Eng.* 19 (2012) 427-465.

[14] L. Dedè, C. Jäggli and A. Quarteroni, Isogeometric numerical dispersion analysis for elastic wave propagation. *Comput. Methods Appl. Mech. Engrg.* 284 (2015) 320-348.

[15] J.A. Evans, Y. Bazilevs, I. Babuška and T.J.R. Hughes, *n*-widths, sup-infs, and optimality ratios for the *k*-version of the isogeometric finite element method. *Comput. Methods Appl. Mech. Engrg.* 198 (2009) 1726-1741.

[16] C. de Falco, A. Reali and R. Vàzquez, GeoPDEs: a research tool for isogeometric analysis of PDEs. *Adv. Eng. Softw.* 42 (2011) 1020-1034.

[17] C. Grossmann, H.G. Roos and M. Stynes, *Numerical Treatment of Partial Differential Equations*, Springer-Verlag, Berlin, 2007.

[18] M.D. Gunzburger, J. Peterson and J.N. Shadid, Reduced-order modeling of time-dependent PDEs with multiple parameters in the boundary data. Comput. Methods Appl. Mech. Engrg. 196 (2007) 1030-1047.

[19] S. Herkt, M. Hinze and R. Pinnau, Convergence analysis of Galerkin POD for linear second order evolution equations. *Electron. Trans. Numer. Anal.* 40 (2013) 321-337.

[20] T. Henri and J.P. Yvon, Stability of the POD and convergence of the POD Galerkin method for parabolic problems, *IRMAR* No 02-40.

[21] P. Holmes, J.L. Lumley and G. Berkooz, *Turbulence, Coherent Structures, Dynamical Systems and Symmetry*, Cambridge Univ. Press, New York, 1996.

[22] T.J.R. Hughes, J. Cottrell and Y. Bazilevs, Isogeometric analysis: CAD, finite elements, NURBS, exact geometry, and mesh refinement. *Comput. Methods Appl. Mech. Engrg.* 194 (2005) 4135-4195.

[23] T.J.R. Hughes, J.A. Evans and A. Reali, Finite element and NURBS approximations of eigenvalue, boundary-value, and initial-value problems. *Comput. Methods Appl. Mech. Engrg.* 272 (2014) 290-320.

[24] T. Iliescu and Z. Wang, Variational multiscale proper orthogonal decomposition: convection dominated convection-diffusion-reaction equations. *Math. Comp.* 82 (2013) 1357-1378.

[25] T. Iliescu and Z. Wang, Are the snapshot difference quotients needed in the proper orthogonal decomposition? *SIAM J. Sci. Comput.* 36 (2014) A1221-A1250.

[26] K. Kunisch and S. Volkwein, Galerkin proper orthogonal decomposition methods for parabolic problems. *Numer. Math.* 90 (2001) 117-148.

[27] K. Kunisch and S. Volkwein, Galerkin proper orthogonal decomposition methods for a general equation in fluid dynamics. *SIAM J. Numer Anal.* 40 (2002) 492-515.

[28] S. Larsson and V. Thomée, *Partial Differential Equations with Numerical Methods*, Springer, 2008.

[29] Z. Luo, J. Chen, I.M. Navon and X. Yang, Mixed finite element formulation and error estimates based on proper orthogonal decomposition for the nonstationary Navier-Stokes equations. *SIAM. J. Numer. Anal.* 47 (2008) 1-19.

[30] L. Piegl and W. Tiller, The NURBS book, Springer-Verlag, New York, 1997.

[31] A. Quarteroni, G. Rozza and A. Manzoni, Certified reduced basis approximation for parametrized partial differential equations and applications. *J. Math. Ind.* 1 (2011) 1-44.

[32] A. Quarteroni and A. Valli, *Numerical Approximation of Partial Differential Problems*, Springer-Verlag, Berlin, 1997.

[33] A. Quarteroni, A. Manzoni and F. Negri, *Reduced Basis Methods for Partial Differential Equations*, Unitext, 92, Springer, 2016.

[34] D. Schillinger, L. Dedè, M.A. Scott, J.A. Evans, M.J. Borden, E. Rank and T.J.R. Hughes, An Isogeometric design-through-analysis methodology based on adaptive hierarchical refinement of NURBS, immersed boundary methods, and T-spline CAD surfaces. Comput. Methods Appl. Mech. Engrg. 249-252 (2012) 116-150.

[35] A. Schmidt, A. Potschka, S. Körkel and H.G. Bock, Derivative-extended POD reduced-order modeling for parameter estimation. *SIAM J. Sci. Comput.* 35 (2013) A2696-A2717.

[36] J. Singler, New POD error expressions, error bounds, and asymptotic results for reduced order models of parabolic PDEs. *SIAM J. Numer. Anal.* 52 (2014) 852-876.

[37] A. Tagliabue, L. Dedè and A. Quarteroni, Isogeometric analysis and error estimates for high order partial differential equations in fluid dynamics, *Comput. Fluids* 102 (2014) 277-303.

[38] T. Taddei, S. Perotto and A. Quarteroni, Reduced basis techniques for nonlinear conservation laws. *ESAIM: M2AN* 49 (2015) 787-814.

[39] S. Volkwein, *Proper Orthogonal Decomposition: Theory and Reduced-Order Mdelling*, Lecture Notes, Universität Konstanz, 2013.

[40] K. Willcox and J. Peraire, Balanced model reduction via the proper orthogonal decomposition. *AIAA* 40 (2002) 2323-2330.

[41] S. Zhu, L. Dedè and A. Quarteroni, Isogeometric analyis and proper orthogonal decomposition for parabolic problems, MATHICSE report, 44.2014 (2014) and MOX report 52.2014 (2014).

MOX Technical Reports, last issues

Dipartimento di Matematica
Politecnico di Milano, Via Bonardi 9 - 20133 Milano (Italy)

10/2016 Flemisch, B.; Fumagalli, A.; Scotti, A.
A review of the XFEM-based approximation of flow in fractured porous media

08/2016 Dassi, F.; Perotto, S.; Si, H.; Streckenbach, T.
A priori anisotropic mesh adaptation driven by a higher dimensional embedding

09/2016 Rizzo, C.B.; de Barros, F.P.J.; Perotto, S.; Oldani, L.; Guadagnini, A.
Relative impact of advective and dispersive processes on the efficiency of POD-based model reduction for solute transport in porous media

07/2016 Pacciarini, P.; Gervasio, P.; Quarteroni, A.
Spectral Based Discontinuous Galerkin Reduced Basis Element Method for Parametrized Stokes Problems

05/2016 Alfio Quarteroni, A.; Lassila, T.; Rossi, S.; Ruiz-Baier, R.
Integrated Heart - Coupling multiscale and multiphysics models for the simulation of the cardiac function

06/2016 Micheletti, S.; Perotto, S.; Signorini, M.
Anisotropic mesh adaptation for the generalized Ambrosio-Tortorelli functional with application to brittle fracture

03/2016 Tarabelloni, N.; Ieva, F.
On Data Robustification in Functional Data Analysis

04/2016 Pettinati, V.; Ambrosi, D; Ciarletta P.; Pezzuto S.
Finite element simulations of the active stress in the imaginal disc of the Drosophila Melanogaster

01/2016 Domanin, M.; Buora, A.; Scardulla, F.; Guerciotti, B.; Forzenigo, L.; Biondetti, P.; Vergara, C.
Computational fluid-dynamic analysis of carotid bifurcations after endarterectomy: closure with patch graft versus direct suture

02/2016 Crivellaro, A.; Perotto, S.; Zonca, S.
Reconstruction of 3D scattered data via radial basis functions by efficient and robust techniques